

# Sub-seasonal behaviour of Asian summer monsoon under a changing climate: assessments using CMIP5 models

Sooraj K P<sup>1</sup>, Pascal Terray<sup>1,2,3</sup> and Prince K Xavier<sup>4</sup>

<sup>1</sup>Centre for Climate Change Research, Indian Institute of Tropical Meteorology,  
Pune 411008, India

<sup>2</sup>Sorbonne Universites (UPMC, Univ Paris 06)-CNRS-IRD-MNHN, LOCEAN Laboratory, 4  
place Jussieu, Paris, France

<sup>3</sup>Indo-French cell for Water Sciences, IISc-IITM-NIO-IRD Joint International Laboratory,  
IITM, Pune 411008, India

<sup>4</sup>Met Office Hadley Centre, FitzRoy Road, Exeter, EX1 3PB, United Kingdom

Climate Dynamics (revised)

Jul, 2015

Corresponding author address:

Sooraj K. P.

Centre for Climate Change Research

Indian Institute of Tropical Meteorology

Pune 411008, India

e-mail: [sooraj@tropmet.res.in](mailto:sooraj@tropmet.res.in)

Numerous global warming studies show the anticipated increase in mean precipitation with the rising levels of carbon dioxide concentration. However, apart from the changes in mean precipitation, the finer details of daily precipitation distribution, such as its intensity and frequency (so called daily rainfall extremes), need to be accounted for while determining the impacts of climate changes in future precipitation regimes. Here we examine the climate model projections from a large set of Coupled Model Inter-comparison Project 5 (CMIP5) models, to assess these future aspects of rainfall distribution over Asian Summer Monsoon (ASM) region. Our assessment unravels a north-south rainfall dipole pattern, with increased rainfall over Indian subcontinent extending into the western Pacific region (north ASM region, NASM) and decreased rainfall over equatorial oceanic convergence zone over eastern Indian Ocean region (south ASM region, SASM). This robust future pattern is well conspicuous at both seasonal and sub-seasonal time scales. Subsequent analysis, using daily rainfall events defined using percentile thresholds, demonstrates that mean rainfall changes over NASM region are mainly associated with more intense and more frequent extreme rainfall events (i.e. above 95<sup>th</sup> percentile). The inference is that there are significant future changes in rainfall probability distributions and not only a uniform shift in the mean rainfall over the NASM region. Rainfall suppression over SASM seems to be associated with changes involving multiple rainfall events and shows a larger model spread, thus making its interpretation more complex compared to NASM. Moisture budget diagnostics generally show that the low-level moisture convergence, due to stronger increase of water vapour in the atmosphere, acts positively to future rainfall changes, especially for heaviest rainfall events. However, it seems that the dynamic component of moisture convergence, associated with vertical motion, shows a strong spatial and rainfall category dependency, sometimes offsetting the effect of the water vapour increase. Additionally, we found that the moisture

54 convergence is mainly dominated by the climatological vertical motion acting on the  
55 humidity changes and the interplay between all these processes proves to play a pivotal role  
56 for regulating the intensities of various rainfall events in the two domains.

57 **Kew words:**

58 Asian summer monsoon; precipitation characteristics; north-south rainfall dipole pattern;  
59 moist mechanisms; daily rainfall extremes

60

## 1. Introduction

Global climate change is no more a scientific curiosity now, as convincing evidences can be found in many facets of the climate system such as temperature increase, snow cover decrease, ice extent and thickness, sea level rise and more frequent extreme events (IPCC 2001, 2007, 2013, 2014). However, determining the regional rainfall response to climate change is much more difficult and challenging (Chou et al. 2009; Bony et al. 2013; Kitoh et al. 2013; Krishnan et al. 2013). Specifically, assessing the potential impact of global climate change on the Asian summer monsoon (ASM) characteristics is a major concern, especially for the densely populated countries in south Asia, like India. This prompts for an imperative assessment of the ASM behaviour in the future changing climate, which is now recognised as a principal challenge for the whole scientific community.

Many previous studies (e.g. Meehl and Washington 1993; Bhaskaran et al. 1995; Douville et al. 2000, 2002; May 2002, 2004, 2011; Turner et al. 2007; Turner and Slingo 2009; Turner and Annamalai 2012) noted that greenhouse warming intensifies the monsoon precipitation over ASM region, particularly over Indo-Bay of Bengal region. A slight poleward shift and a weakening of the low-level monsoon circulation have also been suggested, leading to the so-called “monsoon paradox” (e.g. Turner et al. 2007; May 2004; Cherchi et al. 2011). Recent investigations using Coupled Model Intercomparison Project phase 5 (CMIP5) projections further confirm these inferences (e.g. Menon et al. 2013; Kitoh et al. 2013; Sandeep and Ajayamohan 2015; Sharmila et al. 2015; Sooraj et al. 2015). However, Ma and Yu (2014) and Ogata et al. (2014), using the same CMIP5 projections, highlight again this monsoon paradox with a strengthening of the ASM low-level circulation, but a weaker upper-level circulation. So, while consistent and repeated evidences are found for the future rainfall abundance under different CMIP projections (e.g. May 2002, 2004, 2011; IPCC 2001, 2007, 2013; Turner et al. 2007; Turner and Slingo 2009; Hsu et al. 2012;

Kitoh et al. 1997, 2013; Sooraj et al. 2015), contradictions still prevail for the ASM circulation changes (Ma and Yu 2014; Tanaka et al. 2005; Ueda et al. 2006). Recent ultra-high resolution atmospheric model simulations also show consistency in weakening of large-scale ASM overturning circulation in future projections (Ashfaq et al. 2009; Krishnan et al. 2013). However, these ultra-high resolution models also simulate decreasing summer precipitation over the Western Ghats, one of the key rainfall belts over the Indian monsoon region; the results of which are not consistent with the coarse CMIP5 projections (e.g. Sooraj et al. 2015; Sharmila et al. 2015). Adding further complexity to these, Kitoh et al. (2013) demonstrate strong sensitivity of ASM land rainfall relative to other regional monsoons in a global warming context. The specific reasons for all these discrepancies are not yet clear and hence the future ASM characteristics under global warming scenario remain intriguingly an open question, and still elude us.

The future changes in climate phenomena, such as El Niño Southern Oscillation (ENSO) or Indian Ocean Dipole Mode (IOD), can also modulate future ASM characteristics, as ENSO and IOD are tightly linked to ASM variability (Pillai and Annamalai 2012; Ashok et al. 2001; Ashok et al. 2004; Ummenhofer et al. 2011). Many studies have investigated these aspects (e.g. Ashrit et al. 2005; Yukimoto et al. 2006; Turner et al. 2007; Annamalai et al. 2007; Jourdain et al. 2013). For example, Annamalai et al. (2007) using selected CMIP3 models with a realistic representation of ENSO-monsoon relationship, showed increase in mean monsoon rainfall as well as an increase in interannual variability (by about 5%–10%, compared to the 20<sup>th</sup> century CMIP3 runs). Annamalai et al. (2007) additionally suggested that monsoon-ENSO relationship may not weaken under global warming scenario. Turner et al. (2007), using HadCM3 model configurations, also found that the teleconnection between ENSO and the ASM remains robust in the future climate. According to them, there is increased SST variability over east Pacific, which promotes an increase in monsoon

variability. Some other earlier studies also showed an increase in monsoon rainfall variability in future climate (Hu et al. 2000; May 2004; Yukimoto et al. 2006). Recently, Jourdain et al. (2013) have re-evaluated these aspects using a set of selected CMIP5 models, which show limited biases with regard to monsoon-ENSO relationship. These selected CMIP5 models also consistently produce significantly more summer rainfall over India and South Asian region during the 21<sup>st</sup> century compared to the historical period. On interannual time scales, contrary to the aforesaid results (e.g. Hu et al. 2000; May 2004; Yukimoto et al. 2006), they found no significant changes in monsoon variability in most of these selected models. Therefore, the lack of consensus among the models points that future projection of monsoon variability also remains highly uncertain.

The aforementioned studies (e.g. Turner et al. 2007; Jourdain et al. 2013; Sandeep and Ajayamohan 2015; Sooraj et al. 2015) deciphered future ASM changes using seasonal mean precipitation. However, the finer temporal details of precipitation distribution, such as its intensity and frequency (in other words daily rainfall extremes), are the most important factors in determining the impacts of future changes in precipitation (Meehl et al. 2000; Trenberth 2012). These finer details on rainfall changes cannot be inferred solely using seasonal mean rainfall. Moreover, monsoon daily and intraseasonal variabilities influence the seasonal mean through generation of internal variability and act as major building blocks for ASM (Goswami et al. 2006a; Goswami and Xavier 2005). This, in turn, points to the importance of rainfall frequency and intensity changes in deciphering the physical factors responsible for the ASM trends in future projections. Supporting this argument, some previous observational studies on ASM show that heavy daily precipitation events tend to become more frequent (Goswami et al. 2006b; Rajeevan et al. 2008), while light to moderate events become less frequent (Dash et al. 2009). Recently, Chou et al. (2012) made an attempt to analyse future changes in precipitation characteristics (its intensity and frequency) over the

global tropics ( $30^{\circ}\text{S}$ - $30^{\circ}\text{N}$ ) and also provided possible mechanisms for these changes, using CMIP3 models. However, how global warming exactly affects the ASM precipitation characteristics is less known and the underlying mechanisms are not well understood. The present study intends to address this aspect in the CMIP5 database, taking the intensity and frequency of the future ASM rainfall changes into full consideration. As the intensity and frequency changes can vary geographically as well, we also pay attention to the regional features of future daily rainfall characteristics, concentrating specifically on the detailed physical processes responsible for these changes.

Future changes in seasonal mean ASM rainfall have been studied in Sooraj et al. (2015). The current work is a follow up of this study, extending it to the daily time scale, with a particular focus on daily rainfall extremes. We aim to examine the future changes in precipitation intensity and frequency over a large ASM region ( $50^{\circ}\text{E}$ - $110^{\circ}\text{E}$  and  $20^{\circ}\text{S}$ - $30^{\circ}\text{N}$ ), where large-scale convection dominates with multiple regional rainfall maxima over the eastern equatorial Indian Ocean and central India/north Bay of Bengal, respectively (Annamalai and Sperber 2005). Our future assessment here basically unravels a north-south rainfall dipole pattern positioned over these two regional rainfall centres and is found to occur at both seasonal and sub-seasonal time scales in the CMIP5 projections. This peculiar robust future change signature in a large set of CMIP5 models motivated further to explore the detailed mechanisms that induced these changes. In particular, we focus on changes in precipitation frequency and intensity, and their association with changes in seasonal mean precipitation over ASM. We also aim to pursue the relative contributions of different moisture budget components on the projected regional rainfall changes over ASM region, at sub-seasonal time scale, to provide further insights on the governing physical processes.

The manuscript comprises the following sections. Section 2 includes data and methodology, giving a brief description of the datasets and methodologies used in our

analysis. Section 3 presents the sub-seasonal aspects of monsoon response in climate change experiments. Section 4 examines the possible mechanisms causing the future rainfall patterns. Section 5 provides the discussion and summarizes the main conclusions from our study.

## **2. Data and Methodology**

### **2.1 Data used**

We use the historical and Representative Concentration Pathway (RCP) 4.5 climate experiments from 32 Coupled General Circulation Models (CGCM) contributing to CMIP5 (Taylor et al. 2012; <http://pcmdi9.llnl.gov>). Table 1 provides the model details and descriptions. Out of these 32, there are 12 (see red coloured ones in Table 1) models with the necessary daily atmospheric circulation and precipitation fields for both historical and RCP 4.5 simulations available for a moisture budget analysis, at the time of our analysis. A moisture budget analysis using a larger number of models is currently hampered by the non-availability of all the necessary daily variables for many CMIP5 models. We also use these selected models to further understand the detailed physical process causing the change in rainfall pattern in future climate and to illustrate the inter-model spread in the CMIP5 database in the following sections.

The 20-year mean during 1980-1999 in historical simulations defines the present-day climatology, the mean during 2080-2099 in RCP 4.5 defines the future climatology, and their difference represents the future change under global warming. All the diagnostics are performed only for the boreal summer season (June to September, JJAS hereafter). Note also that we often use the term “sub-seasonal” throughout the manuscript. For avoiding any confusion on its usage, it simply refers to analysis pertaining to daily rainfall.

We also use daily rainfall data from Tropical Rainfall Measuring Mission (TRMM B42 version, Huffman et al. 2007). In the rest of the manuscript, “TRMM” refers to this observed rainfall data. The period of analysis is from 1998 to 2009 for rainfall.



## 2.2 Diagnostic methods for daily rainfall distribution and extremes

As per recent studies (e.g. Kim et al. 2014), state-of-art climate models show a wide spread in simulating the precipitation intensities for the present-day climate and using absolute rainfall thresholds to a group of models may be problematic in distinctly capturing the precipitation strength, as the same precipitation intensity would correspond to a different percentile in different model simulations. In other words, future ASM assessments based on absolute rainfall thresholds may not be sufficient enough within the context of climate change projections. So relying on the spread information inherent in a set of models, here we employed percentile intensity estimates, to identify the daily rainfall extremes in each model separately. For each model (and also observation), the percentile values are calculated for JJAS period of every year and then averaged across the years for estimating the mean value for this particular model. The averaging is used here to eliminate the effects of interannual variations, which are not considered in this study. As an example, we show the computed rainfall intensities corresponding to 90, 95 and 99<sup>th</sup> percentiles for both observations (e.g. TRMM) and historical CMIP5 simulations in Figure 1. One can easily notice that the percentile estimates differ widely among the models, thus demonstrating systematic discrepancies in the precipitation intensities. For example, the rainfall intensity at 99<sup>th</sup> percentile is close to 25 mm day<sup>-1</sup> in CanESM2 (denoted by CAN in Fig. 1), IPSL-CM5A-LR (denoted by IPLR) and BNU-ESM (denoted by BNU), whilst it is around 60 mm day<sup>-1</sup> in BCC-CSM1.1 (see BCC in Fig. 1) and 40 mm day<sup>-1</sup> in CCSM4 (see CCSM in Fig. 1). One can also see that while TRMM shows quite distinct values for 90 and 95<sup>th</sup> percentile estimates (22 and 34 mm day<sup>-1</sup>, respectively), it is not the case in many models (CanESM2, GFDL-ESM-2G, GFDL-ESM-2M, GFDL-CM3, IPSL-CM5A-LR and IPSL-CM5A-MR). As an illustration, GFDL-ESM-2G has very comparable 90 and 95<sup>th</sup> percentile intensities equal to 15 and 18 mm day<sup>-1</sup>, respectively. While other recent studies on future ASM climate (e.g.

Kitoh et al. 2013; Sharmila et al. 2015) used simple “absolute” threshold indices to define the rainfall regimes in the current climate and percentage changes with respect to these absolute thresholds to assess future change, our study, using percentile based thresholds, takes care of the above systematic inconsistencies in the precipitation intensities in order to obtain more robust results for future changes.

Taking account of this large inter-model spread in percentile estimates of precipitation intensity among the models (as noted above in Fig. 1), the extreme events for each model are estimated using their own respective percentile thresholds. Note also that the percentile thresholds for each model are chosen based on their historical simulations, retaining the same thresholds for RCP4.5 simulations to determine future changes. As noted above, the percentile estimates for each model are calculated for JJAS period of every year, before taking their final mean.

In our analysis of the daily rainfall time series of the 32 CMIP5 models listed in Table 1, we use the following percentile thresholds to assess the daily rainfall distribution in historical simulations and its future change in RCP4.5 simulations: 25, 75, 90, 95 and 99<sup>th</sup> percentiles. Previous studies dealing on climate change extremes typically used only the 90<sup>th</sup> percentile as a threshold for defining rainfall extremes (e.g. Moberg et al. 2006; IPCC 2007). As our interest is also on the rainfall extremes, we decide to refine this top 10 % of the daily rainfall distribution into further bins (90, 95 and 99<sup>th</sup> percentiles) in order to provide more spatial details about very intense rainfall events (see Figures 2, 3 and 5 in the following sections). Interestingly, it is found that the 99<sup>th</sup> percentile threshold shows much more inter-model spread compared to the 90 and 95<sup>th</sup> percentiles in the CMIP5 database (see Fig. 1).

However, in order to simplify the discussion about the frequency/intensity of the rainfall events and also the moisture budget analysis, when individual models are considered (e.g. those in red in Table 1), only four precipitation regimes are identified: light, moderate,

heavy and heaviest rainfall events (see Figures 4 and 7-13 in the following sections). Light events are the rainfall events falling within the percentile thresholds of 1 to 25<sup>th</sup>. Similarly, moderate (heavy) events used a percentile threshold interval between 25 to 75<sup>th</sup> (75 to 95<sup>th</sup>) percentiles. Heaviest rainfall events are defined as rainfall events with intensity above the 95<sup>th</sup> percentile threshold. Similar type of percentile threshold analysis can be found in Lau and Wu (2007) and Allan and Soden (2008) for the global tropics, but they used slightly different percentile definitions. For calculating frequency in each rainfall regime, we simply count the number of days for each rainfall event in each category (as defined above) over the region of interest in the entire 20 year, for the JJAS season. Frequency will be expressed in percentage with respect to the total number of JJAS days. On the other hand, the rainfall intensity (in mm day<sup>-1</sup>) is estimated by taking the average rainfall for each category.

Our analysis will focus specifically on extreme precipitation events (identified using the percentile threshold intensity method described above) over the North (60-110°E, 5-25°N) and South (80-110°E, 15°S-Equator) ASM regions (NASM and SASM, respectively, hereafter). These regions basically define the two important heat sources associated with ASM system (Annamalai and Sperber 2005). These regional rainfall centres are found to interact and influence each other on all time scales (Annamalai and Sperber 2005) and may play a vital role to determine the spatio-temporal structure of future ASM response. The reason for selecting these regions for further analysis will become evident as we proceed to the next section.

In order to further document the spatial variability of daily rainfall distributions over ASM domain in present-day and future climates, we also employed two classical statistics, namely skewness and kurtosis coefficients (von Storch and Zwiers 2001). These statistics are computed as

$$Skewness = \frac{nM3}{(n-1)(n-2)\sigma^3} \quad (1)$$

$$Kurtosis = \frac{M_4}{n \sigma^4} - 3 \quad (2)$$

where  $n$  is the number of observations,  $M_3$  ( $M_4$ ) is equal to the sum of the deviations from the mean raised to the third (fourth) power and  $\sigma$  is the standard deviation.

Skewness measures the deviation of the distribution of a variable from symmetry. For a symmetrical distribution, the skewness coefficient is always equal to zero, but the converse is not true. Skewness is zero for a normal distribution. For unimodal distributions shifted to the right (left), the skewness coefficient is positive (negative). Kurtosis measures the flatness or peakedness of the distribution of a variable. The kurtosis coefficient is always greater or equal to -2 and is equal to zero for a normal distribution. In most cases, if the kurtosis is greater (lower) than zero then the distribution is more peaked (flatter) than the normal distribution with the same mean and standard-deviation. Extreme departures from the mean will cause very high values of kurtosis. Consequently, the kurtosis coefficient can be used to detect extreme observations or outliers in a sample of observations. These statistics are applied here to the unfiltered daily rainfall anomalies for each model. The daily anomalies (both the observed and simulated) are calculated by removing the annual cycle composed of the time mean and the first three Fourier harmonics. Finally, skewness and kurtosis statistics, computed separately for each model, are averaged across the models for both the RCP4.5 and historical simulations in order to obtain more robust results.

### 3. Changes in precipitation frequency and intensity

Figures 2a-f depict the ensemble seasonal mean rainfall pattern, along with spatial distributions of sub-seasonal percentile rainfall intensities in the simulated present-day monsoon climate using 32 CMIP5 models. As described earlier, in Figures 2b-f, the percentile rainfall intensities are calculated for each model, for each and every JJAS season, before averaging. The subsequent grand “ensemble mean” (using 32 models) is shown here. Figure 3 displays rainfall statistics from TRMM product using exactly the same method. The

observed seasonal mean rainfall pattern is realistically simulated by the ensemble mean (e.g. compare Figs. 2a and 3a), but with reduced intensity. Consistent with previous studies, the figures also suggest that ASM consists of multiple local rainfall maxima centred over the Bay of Bengal region, the tropical western Pacific and the eastern equatorial Indian Ocean (Annamalai and Sperber 2005; Annamalai and Liu 2005; Annamalai et al. 2007; Sooraj et al. 2015). The seasonal rainfall climatology of CMIP5 models and its biases have been recently documented (Sperber et al. 2013; Sooraj et al. 2015) and are not repeated here for conciseness.

Coming to the sub-seasonal patterns (Figs. 2b-f and 3b-f), the ensemble mean of CMIP5 models overestimates the observed rainfall intensities of lower tail events (which belong to light and moderate events), while underestimating those in the upper tail of the daily rainfall distribution, a common problem in many state-of-art climate models (e.g. Kim et al. 2014; Xavier 2012; Chou et al. 2012; Turner and Slingo 2009). Xavier (2012) while evaluating precipitation distribution in 14 CMIP3 climate models found that most models tend to reside in a light rainfall regime and the transition towards heavy precipitation is not as gradual as in the observations. In the observations (Figs. 3b-f), the contribution of lower tail rain intensities to the seasonal total rainfall appears to be small compared to those intensities above the 90<sup>th</sup> percentile threshold. However for the model ensemble mean, there seems to be significant contributions from all the rainfall categories. All the aforementioned spatial features, particularly sub-seasonal analysis, are seen consistently across the individual models.

In order to illustrate this, Figure 4 displays the behaviour of the 12 selected models (e.g. those in red in Table 1; see Section 2.1 for further details) in simulating the daily rainfall characteristics over the two important regional heat source regions in the ASM domain (e.g. NASM and SASM). Note that we used here only these 12 individual models in order to be

311 consistent with our subsequent discussion using moisture budget estimates (see Section 4). In  
312 both domains, while precipitation intensity (see Figs. 4a-b) rises rapidly from moderate to  
313 heaviest rainfall events (see Section 2.2 for more details on rainfall categories and related  
314 definitions) reaching more than 20 mm day<sup>-1</sup> in most of the models, the rainfall frequency  
315 (expressed in percentage, see Figs. 4c-d) decreases as the intensity increases from light to  
316 heaviest events as expected. Accordingly, light to moderate events are relatively more  
317 frequent in number compared to heavy and heaviest events. Furthermore, the distribution of  
318 precipitation intensity (see Figs. 4a-b) and frequency (expressed in percentage, see Figs. 4c-  
319 d) are generally similar in both domains, with slight exceptions in moderate rain frequency.  
320 But, if we look more carefully at Figures 4a-d, we observe that the models differ among  
321 themselves in simulating the finer details of the daily rainfall distributions. While all the  
322 models show marginal intensity biases for light to heavy rainfall events (see the TRMM  
323 column in Figs. 4a-b, for observations), there is relatively large model spread for the heaviest  
324 rainfall events, with almost all the models systematically underestimating the precipitation  
325 intensity of rainfall events above the 95<sup>th</sup> percentile threshold. Most of the models also  
326 underestimate (overestimate) the frequency of light (moderate) events compared to  
327 observations (see Figs. 4c-d). It seems that the frequency of events in the lower tail is  
328 relatively less well captured compared to the frequency of upper tail events (heavy and  
329 heaviest events) in the coarse CMIP5 models. Recent ultra-high resolution (with 20 km  
330 horizontal resolution) atmospheric model simulations show more realistic representation of  
331 monsoon rainfall intensity and frequency (Krishnan et al. 2013), suggesting the importance of  
332 realistic representation of orography and convective processes for simulating the daily  
333 rainfall distribution over the Indian domain. This points towards the inadequacy of CMIP5  
334 models (being coarser in resolution) in resolving the fine ASM precipitation features  
335 (Krishnan et al. 2013; Sperber et al. 2013; Sooraj et al. 2015) and to problems associated with

the interpolation of the rainfall time series from these models, which is required for computing ensemble means.

We now focus on similar statistics computed from the RCP4.5 simulations. Figure 5 shows the spatial distribution of projected future rainfall changes for the seasonal mean and for the percentiles of daily rainfall distribution. Note here that for each model, the percentiles for the future climate simulations are derived independently of the percentiles estimated from present-day simulations (using exactly by the same method as described in Section 2). The future change of the percentiles is estimated for each model and, finally, the ensemble mean of these differences is computed. Future changes at both the seasonal and sub-seasonal time scales depict a significant north-south dipole-like pattern with increased rainfall over the Indian subcontinent (e.g. NASM) extending into the western Pacific region and decreased rainfall in southeastern Indian Ocean region coinciding with the oceanic convergence zone (e.g. SASM). The subsequent domain oriented analysis using individual models will demonstrate further the robustness of this dipole structure of future rainfall changes.

Interestingly, the aforementioned mean state rainfall changes are mainly associated with future responses in the higher percentiles (e.g. above the 75<sup>th</sup> percentile; see Figs. 5c-f) and thus the more intense rainfall events, suggesting significant changes in the probability distribution of daily rainfall in the ASM region and not only a uniform shift or change of the mean rainfall.

To further assess these probability distributional aspects of future rainfall changes, we examine the skewness and kurtosis statistics (see Section 2.2 for more details) in the historical and RCP4.5 simulations. Figures 6a-b display the ensemble average skewness and kurtosis computed from the 32 CMIP5 models and estimated from the daily rainfall anomalies in the historical simulations. As expected, the daily rainfall distributions are not Gaussian, but highly positively skewed over the whole ASM region in the present-day

climate with relatively lower values over the latitudes encompassing equatorial IO to Indian landmass and high values to its north and south. The maximum values over northwestern desert region, Pakistan and northwestern Australia are particularly notable. The kurtosis statistic (Fig. 6b) also shows highly positive values and similar spatial distribution, further highlighting the non-Gaussian nature of rainfall time series (recall that a Gaussian time series has a kurtosis of zero and a value greater than zero indicates a distribution more peaked than a Gaussian distribution with the same mean and standard-deviation). Furthermore, the extreme positive values of kurtosis over the northwest India-Pakistan region demonstrate the existence of “outliers” (e.g. very intense daily rainfall events) in the daily rainfall distribution simulated by some of the CMIP5 models in its historical simulations, despite the coarse resolution in most of the CMIP5 models.

In future climate, skewness shows remarkable increase over three regions: northwest Australia, SASM region along equatorial convergence zone and another one over the northwest India-Pakistan domain and western Arabian Sea (Fig. 6c). The kurtosis statistic also shows similar pattern of changes in RCP4.5 simulations, pointing to more frequent extreme flood events over both northwest Australia, western maritime continent and, to a lesser extent, the northwest India-Pakistan in future climate (Fig. 6d). The increase over the Pakistan dry region suggests the potential role of global warming in promoting flood episodes over this region in addition to other factors suggested in recent studies (Rasmussen et al. 2015; Priya et al. 2015). Skewness and kurtosis also show an increase over Indian Peninsula, Bangladesh and the core monsoon region in central Indian landmass (74.5-85°E, 16.5-26.5°N, see Figs. 6c and d). The results over the core monsoon region and the north Bay of Bengal are consistent with the observational study of Goswami et al. (2006b). These authors noted an increase in the frequency and intensity of extreme rainfall events using observational record over the same land region. Thus, several regions in the ASM domain



may witness severe and more frequent anomalous rainfall events according to the CMIP5 simulations.

An intriguing feature is that while both the statistics (skewness and kurtosis) are increasing over the NASM and SASM regions in future climate (see Figs. 6c, d), future changes in mean state show a dipole structure, with increased (decreased) rainfall over NASM (SASM) as displayed in Figure 5. We thus now focus on the NASM and SASM domains for a more detailed examination of future changes in precipitation intensity and frequency, using the rainfall categories defined in section 2.2. This analysis will also enable one to appreciate the spread of the individual models in simulating the future climate. First, recall our earlier descriptions in section 2.2, sub-seasonal future changes associated with such rainfall events over the two domains are again measured relative to the percentile thresholds, solely derived from the present-day climate (again for each model on a season-to-season basis). As noted above, here the detailed analysis using individual models is limited to 12 models, so as to be consistent with the moisture budget discussion in section 4.

Figures 7a and c present the future changes in rainfall intensity and frequency over NASM, respectively. All models show seasonal rainfall intensification over NASM (as already noted in Sooraj et al. 2015), with a relative increase ranging from 6 to 15% for the individual models (see Fig. 7a). The projected changes in the intensity of light to heavy events are mostly positive, but very modest relative to the historical runs (see Fig. 7a). Furthermore, the frequency analysis (see Fig. 7c) suggests that the frequency of the light to moderate events only slightly decrease, while heavy events do not show a uniform robust change throughout the models. In contrast, the heaviest events show a large consensus among the models in depicting a consistent and robust relative increase in their intensities (ranging from 5 to 10%, see Fig. 7a) and frequencies (see Fig. 7c), in agreement with the increase of seasonal rainfall. Consequently, for all the selected models, the projected increase in heaviest

events is largely greater than those of the aforementioned light to moderate events. So based on this frequency and intensity analysis, the mean rainfall increase over NASM region is mainly associated with heaviest rainfall events, whose intensity and frequency are projected to increase significantly in the future climate.

In confirmation with the spatial pattern in Figure 5a, all models show a decrease in the seasonal rainfall over SASM region, with a relative decrease ranging from 5 to 25% for individual models (see Fig. 7b). On sub-seasonal time scale, the precipitation intensity consistently weakens for moderate rainfall events in all the models (see Fig. 7b), thus partially accounting for the mean rainfall suppression. Heavy rain events also show similar tendency to decrease in intensity, but not as consistent and high as for moderate events. Heavy events also show a significant decrease in frequency (with only IPSL-CM5A-LR showing no robust changes, see Fig. 7d), while this frequency decrease is less consistent for moderate events with individual models showing either marginally increase or decrease. An interesting observation here is that heaviest events generally show the largest relative increase in intensity with exceptions only in GFDL-CM3 and CSIRO-Mk3.6.0 (showing decreasing tendency, see Fig. 7b). However, the heaviest events are consistently less frequent over the SASM region in almost all the models, offsetting their increase in intensity as far as their effect on the seasonal mean is concerned (see Figs. 7c-d). So the mean rainfall decrease over SASM region is associated with changes involving multiple rainfall events, the relative contribution of which varies from model to model. But some of the models (as described above) show a certain consensus in suggesting that the seasonal mean changes are mainly associated with a combined reduction in moderate and heavy rainfall intensities, despite of the fact that the heaviest rainfall intensities tend to increase their strength in future for most of the models, as pointed out above. Frequency analysis suggests that the mean rainfall decrease may be related to the reduced frequency in heavy to heaviest rain events. All these results are

also fully consistent with the significant positive increase of both the skewness and kurtosis over the SASM region in future climate as illustrated in Figures 6c-d.

In summary, the above analysis shows that there are distinctive differences in the future changes of probability distribution of rainfall characteristics over two domains; however the rainfall change over SASM is more complex to interpret, compared to NASM. The detailed processes leading to these distinct future changes in rainfall characteristics need further examination, as done in the next Section.

#### 4. Possible mechanisms for future changes in ASM daily rainfall characteristics

Having seen the detailed sub-seasonal characteristics of the future rainfall response over ASM system (as described in the previous section), here we will focus on the possible physical processes causing the daily changes in rainfall intensity. Our approach involves the application of vertically integrated water vapour budgets, to bring out the role of different components (horizontal advection, vertical advection and evaporative fluxes) of the moisture budget for the future change in monsoon rainfall. Subsequently, this can give insight into the effect of various processes in contributing to the future intensification or weakening of regional rainfall over ASM. Moisture budget method has been widely used in various recent studies (e.g. Prasanna and Annamalai 2012; Pillai and Annamalai 2012; Xavier et al. 2014) and equation (3) below is the appropriate formulation in the climate change context (Chou et al. 2009, 2012),

$$P' = E' - \overrightarrow{\overline{V'}} \cdot \nabla \overline{q'} - \overline{\omega' \partial_p q'} \quad (3)$$

where the prime and the overbar denote future change and vertical integration through the entire troposphere, respectively;  $P$  represents the precipitation,  $E$  the surface latent heat fluxes,  $\overrightarrow{V}$  the horizontal velocity vector,  $\omega$  the vertical pressure velocity and  $q$  the specific humidity. The specific humidity is converted into energy units ( $\text{W m}^{-2}$ ), assuming that all the

latent heat of evaporation ( $L$ ) is absorbed. Similarly, both  $E$  and  $P$  are converted into energy units ( $\text{W m}^{-2}$ ). On the right hand side of (3), the last two terms represent the future change in moisture advection (horizontal) and moisture convergence, respectively.

The moisture budget estimates presented here are subjected to the following constraints and approximations. The calculation of the moisture budget is not performed on original atmospheric levels and at each time step for each model; rather it is done at interpolated standard pressure levels and using daily outputs only. Also the budget estimates are made over selected regional domains (NASM and SASM), rather than over the entire tropics. All these factors may contribute to errors which may in turn affect the closure of the moisture budget (Chou et al. 2012).

In Figures 8 and 9, we plot the individual terms of the moisture budget for the present-day climate simulations over NASM and SASM, respectively. Note here that the budget estimates are shown separately for each rainfall categories as defined in Section 2.2 and that the residual term of the moisture budget is also shown in each case. These residuals represent various unresolved sub-grid scale processes, such as water vapour storage in the atmosphere and surface boundary effects (Chou et al. 2012). Regarding balancing constraints of the atmospheric moisture budget, Paula and Kummerow (2014) noted that balancing global moisture budgets is a difficult task and this is even more challenging at regional scales. However, for most of the models and all rainfall categories displayed in Figures 8 and 9, residuals are generally smaller compared to the leading budget components, suggesting that the above approximations and related errors may not drastically modify our major conclusions.

In the present day-climate (see Figs. 8-9), it is evident that moist convergence is the leading term of the moisture budget for heavy to heaviest rainfall events over the two domains. On the other hand, over both domains, the positive contribution from moist

convergence in the moisture budget decreases progressively from heavy to light rainfall events, turning out to be the same order as that of the residual term for moderate events and always assuming negative contribution (and also greater than the residual term) for light events. Interestingly, the contribution of evaporation in the moisture budget follows an evolution, which is nearly opposite to the moisture convergence, since evaporation is the leading term of the moisture budget for light to moderate rainfall events and becomes progressively insignificant to account for the occurrence of more intense rainfall events (especially for the heaviest ones). Finally, moisture advection assumes negative values (e.g. dry advection) for all the rainfall categories and it is relatively smaller (larger) for the heavy to heaviest (light to moderate) events (see Figs. 8-9). The role of moisture advection is thus to reduce the rainfall intensity, especially for the light and moderate rainfall events over the two domains.

For heaviest rain events over the two domains, it seems that evaporation and moisture advection approximately cancel out each other, the residual term becoming eventually the second most important term of the moisture budget (see Figs. 8d-9d). Our analysis further reveals that both evaporation and moisture convergence contribute significantly to the moderate rainfall events, with former one dominating the later. Finally, for light rainfall events, as already noted above, the vertical and horizontal components of moisture budget contribute to reduce significantly its intensity (see Figs. 8a-9a). The indication is that convection might not be dominant process for the light rainfall events over the two domains and other processes such as evaporation and boundary layer process could be more important, consistent with previous studies (Chou et al. 2012).

The future changes in moisture budget terms are examined next. Note here that future changes are not shown in percentage unlike earlier plots related to the rainfall intensity changes (e.g. Figs. 7a, b). As future rainfall responses are of distinct nature in the regions of

interest (see section 3), their budget results are discussed separately. Firstly, for conciseness, over NASM, we mainly focus on changes in heaviest rainfall events, which register a highly significant increase in their intensity and frequency characteristics (as described in section 3), to eventually become the main contributor to the future seasonal mean precipitation enhancement (see Figs. 5 and 7a). For light to moderate events (figures not shown), our analysis shows that only evaporation contributes positively to their marginal future increase in all the models, with no substantial favourable role from moisture advection and convergence. For heavy rainfall events, future changes in budget components vary from model to model and hence no robust conclusion can be drawn (figures not shown).

For the heaviest events, as expected, the changes of the contribution due to moisture convergence in the budget assume a similar distribution as that of rainfall intensity changes, across the models (Fig. 10). Interestingly, in many models, it seems that moisture advection injects dry air into NASM region, offsetting the rainfall intensification (except BNU-ESM and IPSL-CM5A-MR), but this effect is too weak in order to counterbalance the strong positive contribution from moisture convergence. There is an additional positive contribution from evaporation as well for some models, but it is also smaller compared to the moisture convergence contribution. Finally, the residual term is less than moisture convergence (the one exception is CCSM4), but still larger than rest of the budget terms and so it additionally contributes to rainfall changes in some of the models (exception in BCC-CSM1.1, CMCC-CMS, IPSL-CM5A-LR, CSIRO-Mk3.6.0 and NorESM1-M).

We now focus on the SASM region, which experiences reduced seasonal rainfall in future climate simulations (see Figs. 5a and 7b). Future changes in moisture budget for light events are not discussed here due to negligible changes in their rainfall intensities (see Fig. 7b). For moderate events, both moisture advection and convergence components contribute to its reduced rainfall intensity, which, as shown earlier, partially explains the seasonal rainfall

decrease in future climate (see Figs. 7b and 11a). However, the contribution of the moisture divergence seems more significant since it is more robust and of greater amplitude across the models. The residual term is also usually smaller than moisture divergence, but in some cases it still contributes to rainfall reduction in moderate rainfall events, with exceptions in BNU-ESM, CMCC-CMS, CCSM4, GFDL-ESM-2G, IPSL-CM5A-LR and CSIRO-Mk3.6.0. On the other hand, evaporative fluxes from equatorial IO (an open ocean basin with no land boundaries to act as barriers) are generally positive and contribute to enhance the rainfall intensity of the moderate events, thus offsetting partially the combined negative effects of the three other components of the budget.

As noted in Section 3, heavy rain events also show similar tendency to decrease in intensity over SASM. Moisture advection and convergence components are responsible for this reduced intensity in 5 models (see Fig. 11b, BCC-CSM1.1, CCSM4, GFDL-ESM-2M, GFDL-CM3 and CSIRO-Mk3.6.0), however the role of the moisture divergence seems to be more consistent and prominent, compared to its advection counterpart (e.g. moisture advection is positive for BCC-CSM1.1 and GFDL-CM3). The role of the residual term is also different from one model to another, assuming large values for some models and the contribution of the evaporative fluxes is usually small in most of the models. Moreover, the contributions of the different terms of the moisture budget exhibit much inter-model spread and switch sign across the models. So for heavy rainfall events over SASM domain, determining the robust features of the moisture budget, which contribute to the simulated changes for future climate, is more complicated because the residual terms are very large for some models.

In the case of heaviest rainfall events, most models show increased intensity over SASM domain (Fig. 11c), moisture convergence is again the main leading contributor to the moisture budget, with a positive effect for most models. The horizontal advection

(evaporation) component of the budget tends always to damp (enhance) the amplitude of the heaviest events over the SASM. But the amplitude of these terms is rather small and they cancel out each other, leading to the dominance of moisture convergence (see Fig. 11c). Note here that for GFDL-CM3 and CSIRO-Mk3.6.0, which show exceptional decrease in heaviest rainfall intensities, moisture convergence (with negative contribution) dominates the other terms, with a secondary contribution from horizontal advection.

Figures 12-13 further reconcile the contributing factors for the future changes in rainfall over ASM region. Figure 12a-f (Figure 13a-f) shows the vertical profile of future changes in specific humidity and vertical velocity, calculated for each rainfall event and each model, over NASM (SASM) regions, respectively. Again, light rainfall is not included here as its characteristics (intensity and frequency, see Fig. 7) show negligible change over both domains. The distribution of moisture changes looks indistinguishable in both domains and is very similar from one rainfall category to another, demonstrating an increase of vapour content in the lower troposphere (see Figs. 12a-c and Figs. 13a-c), as expected from the Clausius-Clapeyron equation. On the other hand, vertical velocity changes show strong spatial and intensity dependencies (see Figs. 12d-f and Figs. 13d-f). In Figures 12 and 13, we also included the mean vertical velocity profile in the present-day climate to ascertain its role and importance, and to further facilitate interpretation of future rainfall changes (see Figs. 12g-i and 13g-i). The characteristics of vertical motion remain identical over two domains with vertical motion assuming stronger magnitudes as precipitation intensity increases from moderate to heaviest. This statement remains true in the future climate, despite the changes described in Figs. 12d-f and 13d-f. Thus the vertical motion shows much intensity dependency over two domains, whereas it is not the case with mean humidity profile (figures not shown).



Figures 12a-c further ascertain that the general increase in rainfall over NASM is driven mainly by increased moisture convergence, associated with the increased water vapour in the atmosphere, directly related to global warming (Bony et al. 2013). However, Figures 12d-f imply reduced ascending motion over NASM and so it seems that the dynamic component of moisture convergence associated with vertical motion changes in the RCP4.5 simulations shows a drying effect in most of the models. The reduced ascending motion is consistent with the weakening of ASM circulation found in climate models (see Section 1, Krishnan et al. 2013; Sooraj et al. 2015). Interestingly, the drying effect shows substantial progression from moderate to heaviest intensities. Recalling our results in Section 3, the heaviest rainfall events show pronounced increase (see Fig. 7a) despite this prominent drying effect thus implying a paradoxical behaviour. This can be understood by carefully interpreting Figures 12g-i, along with the changes depicted in Figure 12a-f. As mentioned above, the mean vertical motion (see Figs. 12g-i) shows substantial strength in extreme heaviest events, relative to moderate and heavy events. This pronounced strength in climatological ascending motion, in conjunction with moisture changes (Fig. 12c), explains this paradox, as this will promote strong moisture convergence in the lower troposphere (see Fig. 10), and to eventually overcome the above drying effect. Note that the moisture convergence, as discussed here, can also be interpreted as a manifestation of the moisture changes acting on climatological ascending motion, in other words, a nonlinear relationship. One can see from Figure 7a that GFDL-CM3 shows only a slight intensification for the heaviest rainfall events compared to other models (see Fig. 7a) and Figure 12f clearly demonstrates that this discrepancy is due to a pronounced relative reduction in vertical motion and the resultant drying affect in this model. Again, the same drying effect (see Figs. 12d-e), with weaker mean ascending motion (see Figs. 12g-h) and the associated weaker moisture convergence (figure not shown) may also explain the negligibly small changes in

moderate to heavy intensities (as shown in section 3, see Fig. 7a) as it may completely nullify the moistening effect due to the increased moisture in the atmosphere (see Figs. 12a-b).

Over SASM region where there is seasonal rainfall suppression (see Fig. 7b), a pronounced weakening of the ascending motion is found, especially for moderate to heavy rainfall events (see Figs. 13d-e). This imparts a strong negative contribution to the moisture convergence due to decreased vertical motion. Further as explained earlier, weaker climatological ascending motion (relative to that of heaviest intensities, see Figs. 13g-i) implies weaker moisture convergence and thus the interaction between these two processes partially explains the significant reduced intensity in local moderate to heavy rainfall events (see Fig. 7b). Note that the changes in vertical motion portray larger spread over SASM compared to NASM, especially for heavy rainfall events (see Figs. 12e-13e). This may also partially explain the significant model spread, as discussed early while describing the budget terms for heavy rainfall intensity (see Fig. 11b). The implication is that the differences in vertical velocity component may add discrepancy for changes in rainfall intensity among the climate models, which may be attributed to the different cumulus parameterization used in climate models (e.g. Chou et al. 2012).

As noted in the previous section, most models demonstrate increased intensity for heaviest rainfall events over the SASM domain, despite mean rainfall suppression (see Fig. 7b). Figures 13c,i extend support to our earlier argument over NASM region, as the drying effect (due to decreased vertical motion, see Fig. 13f) seems to be not strong enough, to counterbalance the moisture convergence associated with moisture change and mean vertical motion (see Figs. 11c, 13c and 13i). In Figure 7b, earlier we also noted reduced heaviest rainfall intensity in GFDL-CM3 and CSIRO-Mk3.6.0. Figure 13f conspicuously further supports our above argument on the adverse and key contribution of the vertical velocity changes to the moisture convergence, as these two outlier models show a highly significant

weakening of upward motion compared to other models, thus accounting for the reduced intensity in their heaviest rainfall events.

As a last note to this section, our analysis shows that changes in moisture convergence are dominated by either changes in atmospheric water vapour content or changes in vertical motion, depending on the rainfall categories and the associated mean profile of vertical velocity. We also note that the mean climatological vertical velocity shows much intensity dependency compared to humidity, as the former one progresses to large values with increase in rainfall intensity. We see that the moisture convergence is usually dominated by the climatological vertical motion acting on the humidity changes and appears to play a critical role for deciphering the future rainfall intensities. In other words, changes in rainfall intensity are mainly determined by the interplay between all these processes.

## **5. Discussion and conclusion**

The climate change pattern detected in this analysis at both the seasonal and sub-seasonal time scales reveals a north-south dipole-like structure, with increased rainfall over NASM region (on Indian subcontinent) extending into the western Pacific region and decreased rainfall over SASM along the equatorial oceanic convergence zone in the CMIP5 projections. This common spatial structure at both seasonal and daily time scales seems robust as it is detected using 32 CMIP5 models. Our study further infers that future daily rainfall changes are associated with more intense rainfall events (i.e. changes in the higher percentiles, above the 75<sup>th</sup> percentile; see Figs 5c-f), suggesting significant changes in the probability distribution of daily rainfall over the ASM region and not a uniform change of the seasonal JJAS mean in the CMIP5 database.

Recently, Sooraj et al. (2015) and Sharmila et al. (2015) also obtained similar future rainfall patterns in seasonal mean ASM precipitation, using selected CMIP5 models that reasonably represent the present-day rainfall climatology over the ASM region. While their

rainfall pattern also identifies rainfall enhancement over NASM region, the rainfall suppression over SASM is not so robust in their analysis. Those studies used a limited number of models in their analysis, which probably may not be able to fully resolve this peculiar rainfall signature (e.g. asymmetric pattern) in the future climate. Intriguingly coinciding with these results, Srivastava and DelSole (2014) also found a similar asymmetric rainfall structure using CMIP5 models, while trying to identify the dominant spatial-temporal mode associated with future change in ASM variability. By applying discriminant analysis to JJAS rainfall anomalies for two types of CMIP5 simulations (pre-industrial control and 21<sup>st</sup> century runs), they concluded that future response is dominated by two dipole modes: one oriented east-west across the maritime continent and other oriented north-south across the ASM region. Interestingly in contrast to the rainfall increase over NASM region, Kitoh et al. (2013) found the largest rainfall intensification over the western Arabian Sea while studying global and regional monsoon in a changing climate. The reason for this discrepancy may be due to the fact that Kitoh et al. (2013) used a longer monsoon season spanning from May to September to define the northern hemisphere summer monsoon and future change is calculated accordingly. On the other hand, the present study uses the JJAS season (see section 2.1) to define the ASM taking into account the following factors: firstly the rainfall season over the regions encompassing Indian landmass begins in early June and secondly the monsoon rainfall during May occurs mostly over the Ocean. So the rainfall pattern as demonstrated in this study may not be directly comparable with their future rainfall patterns.

Our analysis using daily rainfall events (as defined in section 2.2) infers that there are distinctive differences in the future changes of probability distribution of rainfall characteristics over the two domains; however the rainfall change over SASM is more complex to interpret, compared to NASM. We uniquely attribute the mean rainfall increase over NASM region to heaviest rainfall events, the intensity and frequency of which show a

pronounced increase in future projections. Rainfall suppression over SASM shows contributions from multiple rainfall events, but with large inter-model spread. However, some of the models show a combined reduction in moderate and heavy rainfall intensities. Interestingly, even for this subset of models, the intensity of heaviest rainfall events tends to increase over SASM region.

Recently, Chou et al. (2012), when examining future changes in precipitation characteristics over the entire tropics, using CMIP3 models, have noted that heaviest precipitation events occur more frequently, while light to moderate rain events become less frequent. This coincides with our inferences over NASM. In this regard, earlier Trenberth et al. (2003) noted that increase in rainfall intensity needs to be compensated by decrease in frequency (especially for light to moderate rainfall events). Our present findings support all these previous results.

Our moisture budget inferences for NASM region are also broadly in agreement with the results of recent studies, using approximated water vapour budgets (Bony et al. 2013; Sooraj et al. 2015). Our study further substantiates their results using daily rainfall characteristics (e.g. intensity and frequency). Over NASM region where there is future rainfall abundance in CMIP5 simulations, they found competing effects of the thermodynamic (moisture convergence) and dynamic processes (weakened monsoon circulation). According to them, the former component prevailed over the later one and explains the future rainfall intensification in the CMIP5 models. The interpretation is that the offsetting dynamic processes are due to increase in dry static stability of the atmosphere, which tends to reduce the ascending motion and, consequently, counteracts the rainfall intensification. Substantiating their interpretation, the present diagnostics also demonstrate a considerable offset due to the dynamic component, as moisture convergence due to vertical motion shows a drying effect in most of the models, especially for moderate to heavy events

(Figures 12d-f). This weaker low-level moisture convergence due to weaker mean vertical motion (as explained in section 4) probably explains the negligibly small changes in moderate to heavy rainfall intensities over NASM region in future projection, despite of the increased water vapor (see Fig 7a).

Recently, Lee and Wang (2014) while studying the future changes of intensity and area of the global monsoon using CMIP5 model projection also noticed future increase in rainfall over NASM and they attributed it to the significant moisture increase over this region due to the enhanced cyclonic circulation dominating the Eurasia and North Africa, in the future climate. The amplification of moisture, which is partly related to the thermodynamic effect as discussed above, is consistent with those inferred by Sooraj et al. (2015).

For explaining the rainfall suppression over SASM region, Sooraj et al. (2015) argued that, as the thermodynamic component is always positive over climatological ascending regions, the contribution of dynamic component to total rainfall changes must be strongly negative in order to have negative rainfall anomalies in future projections. They further attributed this reduced ascending motion and rainfall suppression to dry air advection. Some of the earlier studies (e.g., Chou et al. 2009; Chou et al. 2012) also showed similar argument for convective-margin zones, while examining future changes in tropical precipitation using CMIP3 models. In section 4, we show that dry air advection also adds to the rainfall reduction over SASM region in addition to moisture divergence. More specifically, we found that the dry advection effect in moderate rainfall events contributes significantly to the overall rainfall suppression over SASM for some of the models (CMCC-CMS, CCSM4, GFDL-ESM-2G, NorESM1-M, GFDL-ESM-2M and CSIRO-Mk3.6.0, see Fig 11a). Similar results hold for heaviest rainfall events as well (i.e. for GFDL-CM3 and CSIRO-Mk3.6.0, see Fig 11c). However, it should be noted that the contribution due to dry advection is not

733 consistent throughout the models, suggesting its relative importance is model dependent and  
734 more modest.

735         Recently, Srivastava and DelSole (2014), while explaining their results on future  
736 mean rainfall structure (as discussed above), argue that large-scale rainfall reduction over  
737 SASM (equatorial IO) is due to the sudden changes in the radiative balance of the  
738 atmosphere. According to them, global warming weakens the net atmospheric radiative  
739 cooling, which stabilizes the atmosphere eventually suppressing the ascending motion. On  
740 similar lines, earlier Bony et al. (2013) argued that the weaker net atmospheric radiative  
741 cooling, associated with the rising levels of carbon dioxide concentration, affects the strength  
742 of the vertical component of the atmospheric circulation. On the other hand, Stowasser et al.  
743 (2009), using GFDL CM2.1 (GFDL model version 2.1) coupled model projections, argued  
744 that the rainfall suppression over equatorial IO is related to the enhanced convection over  
745 equatorial western Pacific, which forces strong subsidence over eastern equatorial IO region.  
746 The relative role of all these different processes is debatable and needs further investigation.

747         It is generally believed that current coarse climate models do not capture well the  
748 precipitation frequency and intensity, particularly for rainfall extremes (e.g. Allan and Soden  
749 2007, 2008; Chou et al. 2007, 2012); a conclusion which is supported by our current  
750 diagnostics as well (see section 3). A few recent studies have reported important deficiencies  
751 in CMIP5 models and their inability to simulate the ASM Rainfall at different time scales due  
752 to coarse resolution or improper convection parameterization (Saha et al. 2014; Sabeerali et  
753 al. 2015). Some other studies, using time slice experiments and very high resolution or  
754 regional AGCMs suggest that Indian summer monsoon rainfall will decrease in future climate  
755 in contradictions with the results using CMIP5 models (Ashfaq et al. 2009; Krishnan et al.  
756 2013). Thus, present global climate models may not be the best tool for assessing the regional  
757 rainfall changes (with proper sign and amplitude) in the future climate due to the important

role of the detailed changes of the vertical motion profiles on the rainfall intensity changes, as highlighted in this study. A natural extension of this work is thus to assess if the future daily rainfall changes documented here are also seen in the regional simulations produced in the framework of the ongoing Coordinated Regional Downscaling Experiment (CORDEX South-Asia, <http://cccr.tropmet.res.in>). However, in all the CMIP5 models, which we analysed, significant increase in heaviest rainfall events is projected in contrast to light to moderate events over NASM region (see section 3). The increase is also noted over northwest India and Pakistan, which already experienced several severe flood events in the last decade (Priya et al. 2015). So, despite the model caveats, the broader consensus within the models is noteworthy.

The extreme daily rainfall events as discussed in this study (see section 3) are inevitably important for ASM system; however ASM rainfall exhibits significant interannual fluctuations (with a standard deviation of about 9 cm day<sup>-1</sup>), thus creating large-scale and persistent droughts or wet conditions, modulating the local daily rainfall distributions over India (e.g. Webster et al. 1998; Goswami and Ajayamohan 2001; Pillai and Annamalai 2012; Sharmila et al. 2015). Recently, Sharmila et al. (2015) using selected CMIP5 models speculated that severity of extended drought and wet events might also increase notably in future climate. So specific consideration needs to be given to the projected daily rainfall changes over the ASM region during anomalous monsoon years. The present work has not addressed this aspect. As a future work, we wish to examine the mean and distribution changes of daily rainfall in this context, by assessing how the daily rainfall probability distribution may be modified specifically during the extreme monsoon years at the interannual time scale (i.e. strong and weak monsoon years) in the future climate.

The rainfall within the monsoon season also possesses variation spanning synoptic to intraseasonal time scales, thus creating spells of active and break events often lasting a few



783 days to weeks (e.g. Goswami and Ajayamohan 2001; Annamalai and Slingo 2001; Turner  
784 and Slingo 2009; Goswami et al. 2006a). Duration, intensity and frequency of these  
785 active/break events contribute to the seasonal mean (e.g. Goswami and Ajayamohan, 2001;  
786 Sperber et al. 2000). So, future changes of the temporal properties of these sub-seasonal  
787 events could also have a vital impact on agricultural practices such as sowing and seeding of  
788 crops. The precise impact of global warming on the active-break statistics remains unknown,  
789 and is also a challenging problem for future research.

790

## Acknowledgements

We sincerely thank Dr. Rajeevan M, Director, Indian Institute of Tropical Meteorology, India for all the support for this research study. We are also thankful to Drs Krishnan R and Mujumdar M for their valuable support in carrying out this research work. Pascal Terray is funded by Institut de Recherche pour le Développement (IRD, France) and this work was done while Pascal Terray was a visiting scientist at IITM. P. Xavier is supported by the Joint DECC/Defra Met Office Hadley Centre Climate Programme (GA01101). We acknowledge the climate modelling groups, the Program for Climate Model Diagnosis and Intercomparison, and the World Climate Research Programme's working Group on coupled modelling, for making available the "CMIP5" multi-model data sets. We also thank the anonymous reviewers for their constructive comments.

## References

- Allan RP, Soden BJ (2007) Large discrepancy between observed and simulated precipitation trends in the ascending and descending branches of the tropical circulation. *Geophys Res Lett* 34:L18705. doi:10.1029/2007GL031460
- Allan RP, Soden BJ (2008) Atmospheric warming and the amplification of precipitation extremes. *Science* 321:1481–1484
- Annamalai H, Liu P (2005) Response of the Asian Summer Monsoon to changes in El Niño properties. *Q J R Meteorol Soc* 131:805–831
- Annamalai H, Slingo JM (2001) Active/break cycles: Diagnosis of the intraseasonal variability of the Asian summer monsoon. *Clim Dyn* 18:85–102.
- Annamalai H, Sperber KR (2005) Regional heat sources and the active and break phases of boreal summer intraseasonal (30–50 day) variability. *J Atmos Sci* 62: 2726–2748
- Annamalai H, Hamilton K, Sperber KR (2007) The South Asian summer monsoon and its relationship with ENSO in the IPCC AR4 simulations. *J Clim* 20:1071–1092
- Ashfaq M, Shi Y, Tung WM, Trapp RJ, Gao X, Pal JS, Diffenbaugh NS (2009) Suppression of south Asian summer monsoon precipitation in the 21<sup>st</sup> century. *Geophys Res Lett* 36: L01704. doi:10.1029/2008GL036500
- Ashok K, Guan Z, Saji NH, Yamagata T (2004) Individual and combined influences of ENSO and the Indian Ocean dipole on the Indian summer monsoon. *J Clim* 17(16):3141–3155
- Ashok K, Guan Z, Yamagata T (2001) Impact of the Indian Ocean dipole on the relationship between the Indian monsoon rainfall and ENSO. *Geophys Res Lett* 28(23):4499–4502
- Ashrit RG, Kitoh A, Yukimoto S (2005) Transient response of ENSO–monsoon teleconnection in MRI-CGCM2.2 climate change simulations. *J Meteorol Soc Jpn* 83: 273–291

828 Bhaskaran B, Mitchell JFB, Lavery JR, Lal M (1995) Climatic response of the Indian  
829 subcontinent to doubled CO<sub>2</sub> concentration. *Int J Climatol* 15:873–892

830 Bony S, Bellon G, Klocke D, Sherwood S, Fermepin S, Denvil S (2013) Robust direct effect  
831 of carbon dioxide on tropical circulation and regional precipitation. *Nature Geosci*  
832 6:447–451

833 Cherchi A, Alessandri A, Masina S, Navarra A (2011) Effects of increased CO<sub>2</sub> on  
834 monsoons. *Clim Dyn* 37:83–101. doi:10.1007/s00382-010-0801-7

835 Chou C, Tu JY, Tan PH (2007) Asymmetry of tropical precipitation change under global  
836 warming. *Geophys Res Lett* 34:L17708. doi:10.1029/2007GL030327

837 Chou C, Neelin JD, Chen CA, Tu JY (2009) Evaluating the “rich-get-richer” mechanism in  
838 tropical precipitation change under global warming. *J Clim* 22:1982–2005

839 Chou C, Chen CA, Tan PH, Chen KT (2012) Mechanisms for Global Warming Impacts on  
840 Precipitation Frequency and Intensity. *J Clim* 25:3291–3306

841 Dash SK, Kulkarni MA, Mohanty UC, Prasad K (2009) Changes in the characteristics of rain  
842 events in India. *J Geophys Res* 114:D10109

843 Douville H, Chauvin F, Planton S, Royer JF, Salas-Melia D, Tyteca S (2002) Sensitivity of  
844 the hydrological cycle to increasing amounts of greenhouse gases and aerosols. *Clim*  
845 *Dyn* 20:45–68

846 Douville H, Royer JF, Polcher J, Cox P, Gedney N, Stephenson DB, Valdes PJ (2000) Impact  
847 of doubling CO<sub>2</sub> on the Asian summer monsoon: robust versus model-dependent  
848 responses. *J Meteorol Soc Jpn* 78:421–439

849 Goswami BN, Ajayamohan RS (2001) Intraseasonal oscillations and interannual variability  
850 of the Indian summer monsoon. *J Clim* 14:1180–1198

851 Goswami BN, Xavier PK (2005) Dynamics of ‘Internal’ interannual variability of Indian  
852 Summer Monsoon in a GCM. *J Geophys Res* 110:D24104

853 Goswami BN, Wu G, Yasunari T (2006a) The annual cycle, intraseasonal oscillations and  
854 roadblock to seasonal predictability of the Asian summer monsoon. *J Clim* 19:5078–  
855 5099

856 Goswami BN, Venugopal V, Sengupta D, Madhusoodanan MS, Xavier PK (2006b)  
857 Increasing Trend of Extreme Rain Events Over India in a Warming Environment.  
858 *Science* 314:1442–1445

859 Hsu PC, Li T, Luo JJ, Murakami H, Kitoh A, Zhao M (2012) Increase of global monsoon  
860 area and precipitation under global warming: a robust signal? *Geophys Res Lett*  
861 39:L0670. doi:10.1029/2012GL051037

862 Hu ZZ, Latif M, Roeckner E, Bengtsson L (2000) Intensified Asian summer monsoon and its  
863 variability in a coupled model forced by increasing greenhouse gas concentrations.  
864 *Geophys Res Lett* 27:2681–2684

865 Huffman GJ, Adler RF, Bolvin DT, Gu G, Nelkin EJ, Bowman KP, Hong Y, Stocker EF,  
866 Wolff DB (2007) The TRMM Multi-satellite precipitation analysis: quasi global, multi-  
867 year, combined-sensor precipitation estimates at fine scale. *J Hydrometeor* 8:38–55

868 IPCC (2001) Third Assessment Report of the Intergovernmental Panel on Climate Change,  
869 [www.ipcc.ch/ipccreports/ar4-wg1.htm](http://www.ipcc.ch/ipccreports/ar4-wg1.htm)

870 IPCC (2007) Fourth Assessment Report of the Intergovernmental Panel on Climate Change,  
871 [www.ipcc.ch/ipccreports/ar4-wg1.htm](http://www.ipcc.ch/ipccreports/ar4-wg1.htm)

872 IPCC (2013) Fifth Assessment Report of the Intergovernmental Panel on Climate Change,  
873 [www.ipcc.ch/ipccreports/ar4-wg1.htm](http://www.ipcc.ch/ipccreports/ar4-wg1.htm)

874 IPCC (2014) Fifth Assessment Report of the Intergovernmental Panel on Climate Change,  
875 [www.ipcc.ch/ipccreports/ar4-wg1.htm](http://www.ipcc.ch/ipccreports/ar4-wg1.htm)

876 Jourdain NC, Gupta AS, Taschetto AS, Ummenhofer CC, Moise AF, Ashok K (2013) The  
 877 Indo-Australian monsoon and its relationship to ENSO and IOD in reanalysis data and  
 878 the CMIP3/CMIP5 simulations. *Clim Dyn*. doi:10.1007/s00382-013-1676-1  
 879 Kim D, co-authors (2014) Process-Oriented MJO Simulation Diagnostic: Moisture  
 880 Sensitivity of Simulated Convection. *J Clim* 27:5379–5395  
 881 Kitoh A, Yukimoto S, Noda A, Motoi T (1997) Simulated changes in the Asian summer  
 882 monsoon at times of increased atmospheric CO<sub>2</sub>. *J Meteorol Soc Jpn* 75:1019–1031  
 883 Kitoh A, Endo H, Krishna Kumar K, Cavalcanti IFA, Goswami P, Zhou T (2013) Monsoons  
 884 in a changing world: A regional perspective in a global context. *J Geophys Res* 118:  
 885 3053–3065  
 886 Krishnan R, Sabin TP, Ayantika DC, Sugi M, Kitoh A, Murakami H, Turner A, Slingo JM,  
 887 Rajendran K (2013) Will the South Asian monsoon overturning circulation stabilize any  
 888 further? *Clim Dyn* doi:10.1007/s00382-012-1317-0  
 889 Lau KM, Wu HT (2007) Detecting trends in tropical rainfall characteristics, 1979–2003. *Int J*  
 890 *Climatol* 27:979–988  
 891 Lee JY, Wang B (2014) Future change of global monsoon in the CMIP5. *Clim Dyn* 42:101–  
 892 119. doi:10.1007/s00382-012-1564-0  
 893 Ma J, Yu JY (2014) Paradox in the South Asian summer monsoon circulation change: Lower  
 894 tropospheric strengthening and upper tropospheric weakening. *Geophys Res Lett* 41.  
 895 doi: 10.1002/2014GL059891  
 896 May W (2002) Simulated changes of the Indian summer monsoon under enhanced  
 897 greenhouse gas conditions in a global time-slice experiment. *Geophys Res Lett* 29.  
 898 doi:10.1029/2001GL013808

899 May W (2004) Simulation of the variability and extremes of daily rainfall during the Indian  
 900 summer monsoon for present and future times in a global time-slice experiment. *Clim*  
 901 *Dyn* 22:183–204

902 May W (2011) The sensitivity of the Indian summer monsoon to a global warming of 2°C  
 903 with respect to pre-industrial times. *Clim Dyn* 37:1843–1868. doi:10.1007/s00382-010-  
 904 0942-8

905 Meehl GA, Washington WM (1993) South Asian summer monsoon variability in a model  
 906 with a doubled atmospheric carbon-dioxide concentration. *Science* 260:1101–1104

907 Meehl GA, Zwiers F, Evans J, Knutson T, Mearns L, Whetton P (2000) Trends in extreme  
 908 weather and climate events: issues related to modelling extremes in projections of future  
 909 climate change. *Bull Am Me Soc* 81:427–436

910 Menon A, Levermann A, Schewe J, Lehmann J, Frieler K (2013) Consistent increase in  
 911 Indian monsoon rainfall and its variability across CMIP-5 models. *Earth Syst Dynam*  
 912 *Discuss* 4:287–300. doi:10.5194/esdd-4-287-2013

913 Moberg A, co-authors (2006) Indices for daily temperature and precipitation extremes in  
 914 Europe analyzed for the period 1901–2000. *J Geophys Res* 111 (D22).  
 915 doi:10.1029/2006JD007103

916 Ogata T, Ueda H, Inoue T, Hayasaki M, Yoshida A, Watanabe S, Kira M, Ooshiro M, Kumai  
 917 A (2014) Projected Future Changes of the Asian Monsoon: A Comparison of CMIP3  
 918 and CMIP5 model results. *J Meteorol Soc Jpn* 92:207–225

919 Paula JB, Kummerow CD (2014) An Assessment of Atmospheric Water Budget Components  
 920 over Tropical Oceans. *J Clim* 27:2054–2071

921 Pillai PA, Annamalai H (2012) Moist dynamics of severe monsoons over South Asia: Role of  
 922 the tropical SST. *J Atmos Sci* 69:97–115

923 Prasanna V, Annamalai H (2012) Moist dynamics of extended monsoon breaks over South  
 924 Asia. *J Clim* 25:3810–3831

925 Priya P, Mujumdar M, Sabin TP, Terray P, Krishnan R (2015) Impacts of Indo-Pacific sea  
 926 surface temperature anomalies on the summer monsoon circulation and heavy  
 927 precipitation over northwest India-Pakistan region during 2010. *J Clim* 28:3714–3730.  
 928 doi: 10.1175/JCLI-D-14-00595.1

929 Rajeevan M, Bhate J, Jaswal AK (2008) Analysis of variability and trends of extreme  
 930 rainfall events over India using 104 years of gridded daily rainfall data. *Geophys Res*  
 931 *Lett* 35:L18707. doi: 10.1029/2008GL035143

932 Rasmussen KL, Hill AJ, Toma VE, Zuluaga MD, Webster PJ, Houze Jr RA (2015)  
 933 Multiscale analysis of three consecutive years of anomalous flooding in Pakistan. *Q J R*  
 934 *Meteorol Soc* 141:1259–1276. doi: 10.1002/qj.2433

935 Sabeerali C, Rao SA, Dhakate A, Salunke K, Goswami B (2015) Why ensemble mean  
 936 projection of south Asian monsoon rainfall by CMIP5 models is not reliable? *Clim Dyn*  
 937 45:161-174

938 Saha A, Ghosh S, Sahana AS, Rao EP (2014) Failure of CMIP5 climate models in simulating  
 939 post-1950 decreasing trend of Indian monsoon. *Geophys Res Lett* 41:7323-7330.  
 940 doi:10.1002/2014GL061573

941 Sandeep S, Ajaya Mohan RS (2015) Poleward shift in Indian summer monsoon low level  
 942 Jetstream under global warming. *Clim Dyn* 45:337–351. doi 10.1007/s00382-014-2261-  
 943 y

944 Sharmila S, Joseph S, Sahai AK, Abhilash S, Chattopadhyay R (2015) Future projection of  
 945 Indian summer monsoon variability under climate change scenario: An assessment  
 946 from CMIP5 climate models. *Glob Planet Chang* 124:62–78



947 Sooraj KP, Terray P, Mujumdar M (2015) Global warming and the weakening of the Asian  
 948 summer monsoon circulation: Assessments from the CMIP5 models. *Clim Dyn*  
 949 45:233–252. doi:10.1007/s00382-014-2257-7

950 Sperber KR, Slingo JM, Annamalai H (2000) Predictability and the relationship between  
 951 subseasonal and interannual variability during the Asian summer monsoons. *Q J R*  
 952 *Meteorol Soc* 126:2545–2574

953 Sperber KR, Annamalai H, Kang IS, Kitoh A, Moise A, Turner AG, Wang B, Zhou T (2013)  
 954 The Asian summer monsoon: An intercomparison of CMIP5 vs. CMIP3 simulations of  
 955 the late 20<sup>th</sup> century. *Clim Dyn* 41:2711–2744. doi:10.1007/s00382-012-1607-6

956 Srivastava A, DelSole T (2014) Robust Forced Response in South Asian Summer Monsoon  
 957 in a Future Climate. *J Clim* 27:7849–7860

958 Stowasser M, Annamalai H, Hafner J (2009) Response of the South Asian summer monsoon  
 959 to global warming: mean and synoptic systems. *J Clim* 22:1014–1036

960 Tanaka HL, Ishizaki N, Nohara D (2005) Intercomparison of the intensities and trends of  
 961 Hadley, Walker and monsoon circulations in the global warming projections. *Sci Online*  
 962 *Lett Atmos* 1:77–80. doi:10.2151/sola.2005-021

963 Taylor KE, Stouffer RJ, Meehl GA (2012) An overview of CMIP5 and the experiment  
 964 design. *Bull Amer Meteor Soc* 93:485–498

965 Trenberth KE (2012) Framing the way to relate climate extremes to climate change. *Climatic*  
 966 *Change* 115(2):283–290. doi:10.1007/s10584-012-0441-5

967 Trenberth KE, Dai A, Rasmussen RM, Parsons DB (2003) The changing character of  
 968 precipitation. *Bull Amer Meteor Soc* 84:1205–1217 doi:10.1175/BAMS-84-9-1205.

969 Turner AG, Annamalai H (2012) Climate change and the South Asian summer monsoon.  
 970 *Nature Clim Change*. doi:10.1038/NCLIMATE1495

971 Turner AG, Slingo JM (2009) Uncertainties in future projections of extreme precipitation in  
 972 the Indian monsoon region. *Atmos Sci Lett* 10:152–158. doi:10.1002/asl.223  
 973 Turner AG, Inness PM, Slingo JM (2007) The effect of doubled CO<sub>2</sub> and model basic state  
 974 biases on the monsoon-ENSO system. I: mean response and interannual variability.  
 975 *QJR Meteorol Soc* 133:1143–1157  
 976 Ueda H, Iwai A, Kuwako K, Hori ME (2006) Impact of anthropogenic forcing on the Asian  
 977 summer monsoon as simulated by eight GCMs. *Geophys Res Lett* 33:L06703.  
 978 doi:10.1029/2005GL025336  
 979 Ummenhofer CC, Sen Gupta A, Li Y, Taschetto AS, England MH (2011) Multi-decadal  
 980 modulation of the El Nino–Indian monsoon relationship by Indian Ocean variability.  
 981 *Environ Res Lett* 6:034006  
 982 Von Storch H, Zwiers FW (2001) *Statistical Analysis in Climate Research*. Cambridge  
 983 University press. Cambridge UK. Chapter 13. 484 pp.  
 984 Webster PJ, Magaña VO, Palmer TN, Shukla J, Tomas RA, Yanai M, Yasunari T (1998)  
 985 Monsoons: Processes, predictability, and the prospects for prediction. *J Geophys Res*  
 986 103:14451–14510  
 987 Xavier PK (2012) Intraseasonal convective moistening in CMIP3 models. *J Clim* 25:2569–  
 988 2577  
 989 Xavier PK, Raizan R, Wee KC, Emily W (2014) Influence of Madden-Julian Oscillation on  
 990 South East Asia rainfall extremes - Observations and predictability. *Geophys Res Lett*  
 991 41:4406–4412. doi:10.1002/2014GL060241  
 992 Yukimoto S, Noda A, Uchiyama T, Kusunoki S (2006) Climate change of the twentieth  
 993 through twenty-first centuries simulated by MRI-CGCM2.3. *Pap Meteor Geophys* 56:  
 994 9–24  
 995

## Figure Captions

Fig 1: Percentile rainfall intensity for daily time series over the ASM region (60-110°E and 15°S-25°N) from TRMM and historical simulations for selected CMIP5 models. Here BCC stands for BCC-CSM1.1, similarly CMS for CMCC-CMS, BNU for BNU-ESM, CAN for CanESM2, CCSM for CCSM4, GF2G for GFDL-ESM-2G, GF2M for GFDL-ESM-2M, GFCM for GFDL-CM3, IPLR for IPSL-CM5A-LR, IPMR for IPSL-CM5A-MR, CSIR for CSIRO-Mk3.6.0, and finally NOR for NorESM1-M. Note that a log scale is used for the vertical axis and that the unit for this axis is in  $\text{mm day}^{-1}$ .

**Figure 2:** (a) Ensemble mean rainfall (in  $\text{mm day}^{-1}$ ) at seasonal time scale (for JJAS period) for historical simulations using 32 CMIP5 models. (b) to (f) Ensemble mean of rainfall intensities (in  $\text{mm day}^{-1}$ ) at different percentile thresholds using daily rainfall from historical simulations of 32 CMIP5 models, for the JJAS period. See Section 2 for further details about the percentile thresholds definitions.

**Figure 3:** Same as Fig 2, but for TRMM rainfall observations.

**Figure 4a-d:** Rainfall intensity of various rainfall events over (a) NASM and (b) SASM domains, for historical simulations using 12 CMIP5 models. (c) and (d) are same as (a) and (b), but for rainfall frequency. Here BCC stands for BCC-CSM1.1, similarly CMS for CMCC-CMS, BNU for BNU-ESM, CAN for CanESM2, CCSM for CCSM4, GF2G for GFDL-ESM-2G, GF2M for GFDL-ESM-2M, GFCM for GFDL-CM3, IPLR for IPSL-CM5A-LR, IPMR for IPSL-CM5A-MR, CSIR for CSIRO-Mk3.6.0, and, finally, NOR for NorESM1-M. The unit for intensity is in  $\text{mm day}^{-1}$ , while for frequency, it is in percentages.

**Figure 5:** Same as that of Figure 2, but for the future rainfall changes. As explained in the text, the rainfall intensities at various percentile thresholds are derived independently for the historical and RCP4.5 simulations and future change is finally calculated. See the text for more details. Stippling denotes the regions of statistically significant values at the 90%

confidence level, using a two tailed student  $t$ -test for the differences of means using a number of degrees of freedom (DOF) of 62 (e.g.  $\text{DOF}=2\times\text{number of models} - 2$ ). In other words, each model is assumed to be an independent observation for computing the  $t$ -statistic. Color shading represents the future changes values, without applying any significance test. The thick black contour is the zero isoline.

**Figure 6:** Ensemble mean patterns and their future changes for Kurtosis (a and c) and Skewness (b and d) statistics of rainfall distribution, using 32 CMIP5 models. (a) and (b) for present-day climate. (c) and (d) for future change, expressed in percentages.

**Figure 7a-d:** Future change in rainfall intensity (in %) of various rainfall events over (a) NASM and (b) SASM domains. In (c) and (d), same as (a) and (b), but for rainfall frequency (in %). Here BCC stands for BCC-CSM1.1, similarly CMS for CMCC-CMS, BNU for BNU-ESM, CAN for CanESM2, CCSM for CCSM4, GF2G for GFDL-ESM-2G, GF2M for GFDL-ESM-2M, GFCM for GFDL-CM3, IPLR for IPSL-CM5A-LR, IPMR for IPSL-CM5A-MR, CSIR for CSIRO-Mk3.6.0, and, finally, NOR for NorESM1-M.

**Figure 8a-d:** Moisture Budget terms (in  $\text{W m}^{-2}$ ) over NASM region for the present-day climate, as calculated for various rainfall events. MoiCon represents moisture convergence, MoiAdv is for moisture advection, Evap is for evaporation and Res stands for budget residual term. Here BCC stands for BCC-CSM1.1, similarly CMS for CMCC-CMS, BNU for BNU-ESM, CAN for CanESM2, CCSM for CCSM4, GF2G for GFDL-ESM-2G, GF2M for GFDL-ESM-2M, GFCM for GFDL-CM3, IPLR for IPSL-CM5A-LR, IPMR for IPSL-CM5A-MR, CSIR for CSIRO-Mk3.6.0, and, finally, NOR for NorESM1-M.

**Figure 9a-d:** Moisture Budget terms (in  $\text{W m}^{-2}$ ) over SASM region for the present-day climate, as calculated for various rainfall events. MoiCon represents moisture convergence, MoiAdv is for moisture advection, Evap is for evaporation and Res stands for budget residual term. Here BCC stands for BCC-CSM1.1, similarly CMS for CMCC-CMS, BNU for BNU-

ESM, CAN for CanESM2, CCSM for CCSM4, GF2G for GFDL-ESM-2G, GF2M for GFDL-ESM-2M, GFCM for GFDL-CM3, IPLR for IPSL-CM5A-LR, IPMR for IPSL-CM5A-MR, CSIR for CSIRO-Mk3.6.0, and, finally, NOR for NorESM1-M.

**Figure 10:** Future changes in moisture Budget terms (in  $\text{W m}^{-2}$ ) over NASM region as calculated for heaviest rainfall intensities. MoiCon represents moisture convergence, MoiAdv is for moisture advection, Evap is for evaporation and Res stands for budget residual term. Here, BCC stands for BCC-CSM1.1, similarly, CMS for CMCC-CMS, BNU for BNU-ESM, CAN for CanESM2, CCSM for CCSM4, GF2G for GFDL-ESM-2G, GF2M for GFDL-ESM-2M, GFCM for GFDL-CM3, IPLR for IPSL-CM5A-LR, IPMR for IPSL-CM5A-MR, CSIR for CSIRO-Mk3.6.0, and, finally, NOR for NorESM1-M.

**Figure 11a-c:** Future changes in moisture Budget terms (in  $\text{W m}^{-2}$ ) over SASM region as calculated for various rainfall events. MoiCon represents moisture convergence, MoiAdv is for moisture advection, Evap is for evaporation and Res stands for budget residual term. Here, BCC stands for BCC-CSM1.1, similarly CMS for CMCC-CMS, BNU for BNU-ESM, CAN for CanESM2, CCSM for CCSM4, GF2G for GFDL-ESM-2G, GF2M for GFDL-ESM-2M, GFCM for GFDL-CM3, IPLR for IPSL-CM5A-LR, IPMR for IPSL-CM5A-MR, CSIR for CSIRO-Mk3.6.0, and, finally, NOR for NorESM1-M.

**Figure 12a-f:** (a)-(f) Vertical profiles of future change in specific humidity (left panels,  $\times 10^{-3} \text{ kg kg}^{-1}$ ) and vertical component of velocity (middle panels,  $\times 10^{-2} \text{ Pa s}^{-1}$ ) over NASM, as calculated for various rainfall events in 12 selected CMIP5 models. (g)-(i) Mean vertical profiles of vertical component of velocity (unit is  $10^{-2} \text{ Pa s}^{-1}$ ) computed from historical simulations of the same 12 CMIP5 models, for various rainfall events over NASM.

**Figure 13a-f:** (a)-(f) Vertical profiles of future change in specific humidity (left panels,  $\times 10^{-3} \text{ kg kg}^{-1}$ ) and vertical component of velocity (middle panels,  $\times 10^{-2} \text{ Pa s}^{-1}$ ) over SASM, as calculated for various rainfall events in 12 selected CMIP5 models. (g)-(i) Mean vertical

1071 profiles of vertical component of velocity (unit is  $-10^{-2}$  Pa s<sup>-1</sup>) computed from historical  
1072 simulations of the same 12 CMIP5 models, for various rainfall events over SASM.  
1073

1074 **Table Captions:**

1075 **Table 1:** Description of the 32 CMIP5 models used in our analysis. The 12 models shown in  
1076 red are those used for our detailed analysis and those having all the necessary daily  
1077 atmospheric circulation and precipitation fields in both historical and RCP45 simulations, for  
1078 conducting moisture budget analysis.

1079

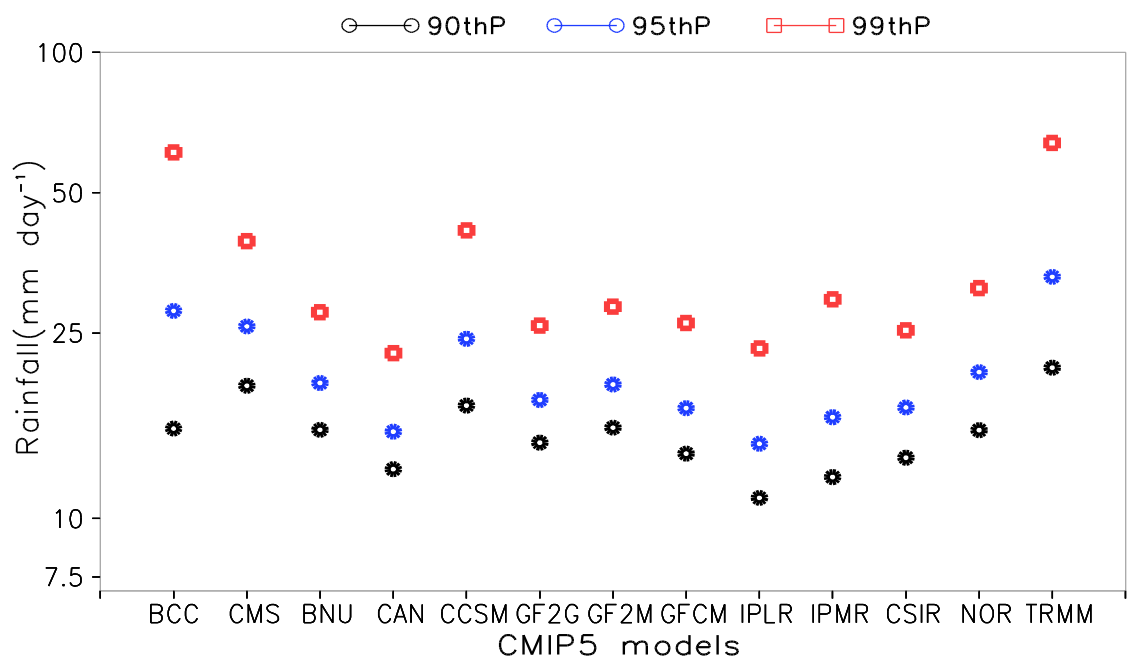
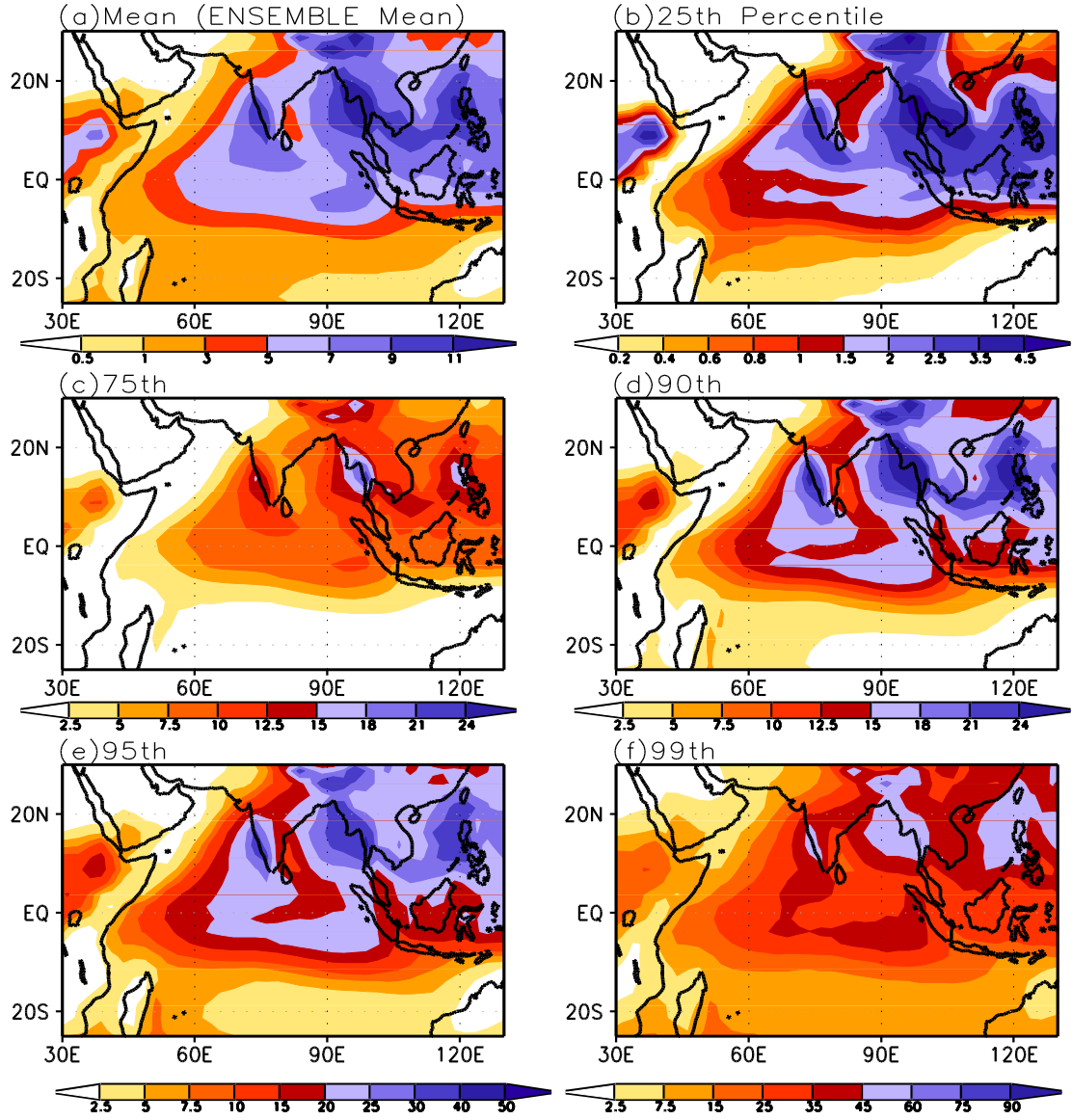
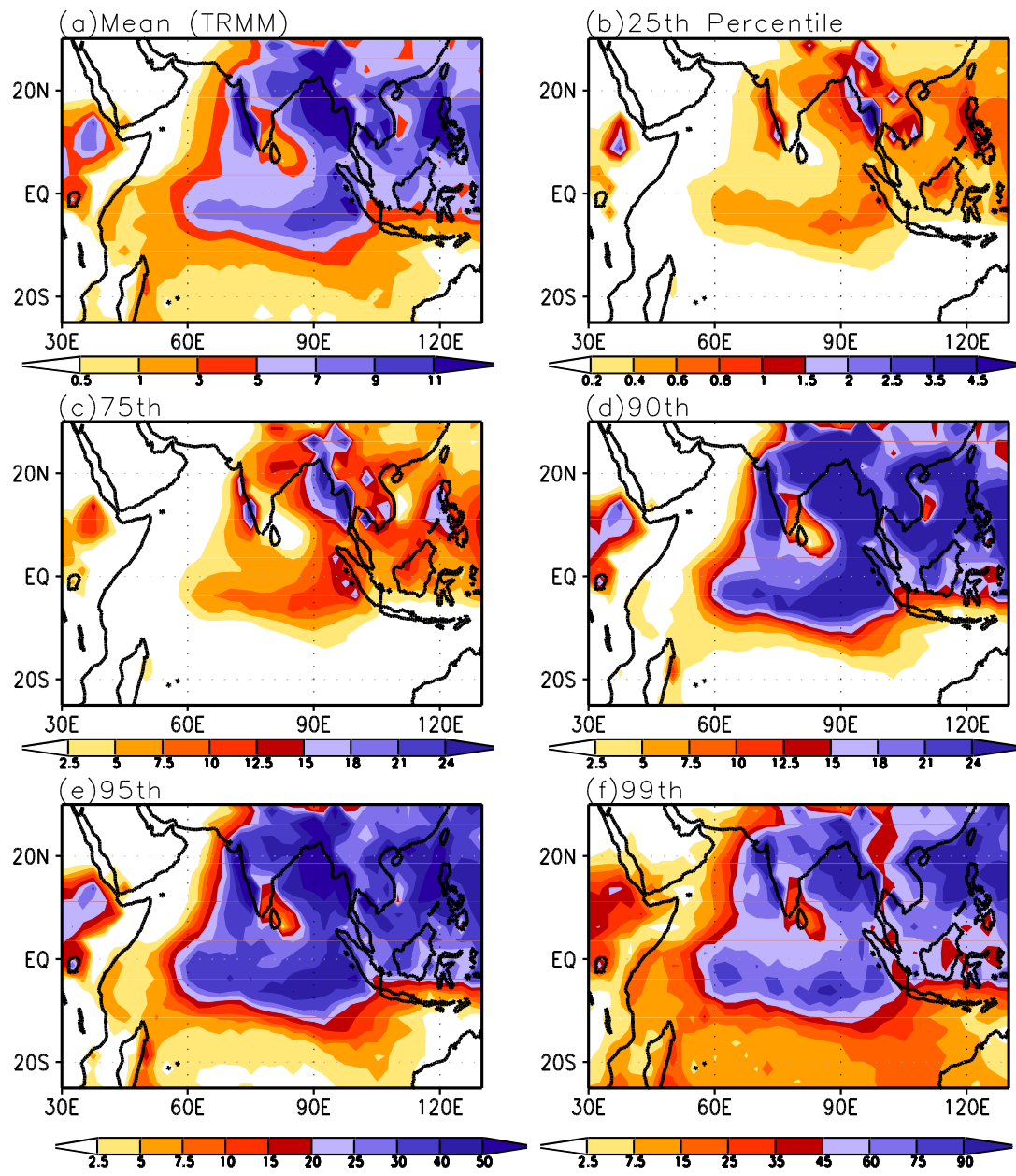


Fig 1: Percentile rainfall intensity for daily time series over the ASM region (60-110°E and 15°S-25°N) from TRMM and historical simulations for selected CMIP5 models. Here BCC stands for BCC-CSM1.1, similarly CMS for CMCC-CMS, BNU for BNU-ESM, CAN for CanESM2, CCSM for CCSM4, GF2G for GFDL-ESM-2G, GF2M for GFDL-ESM-2M, GFCM for GFDL-CM3, IPLR for IPSL-CM5A-LR, IPMR for IPSL-CM5A-MR, CSIR for CSIRO-Mk3.6.0, and finally NOR for NorESM1-M. Note that a log scale is used for the vertical axis and that the unit for this axis is in mm day<sup>-1</sup>.





**Figure 2:** (a) Ensemble mean rainfall (in mm day<sup>-1</sup>) at seasonal time scale (for JJAS period) for historical simulations using 32 CMIP5 models. (b) to (f) Ensemble mean of rainfall intensities (in mm day<sup>-1</sup>) at different percentile thresholds using daily rainfall from historical simulations of 32 CMIP5 models, for the JJAS period. See Section 2 for further details about the percentile thresholds definitions.



**Figure 3:** Same as Fig 2, but for TRMM rainfall observations.

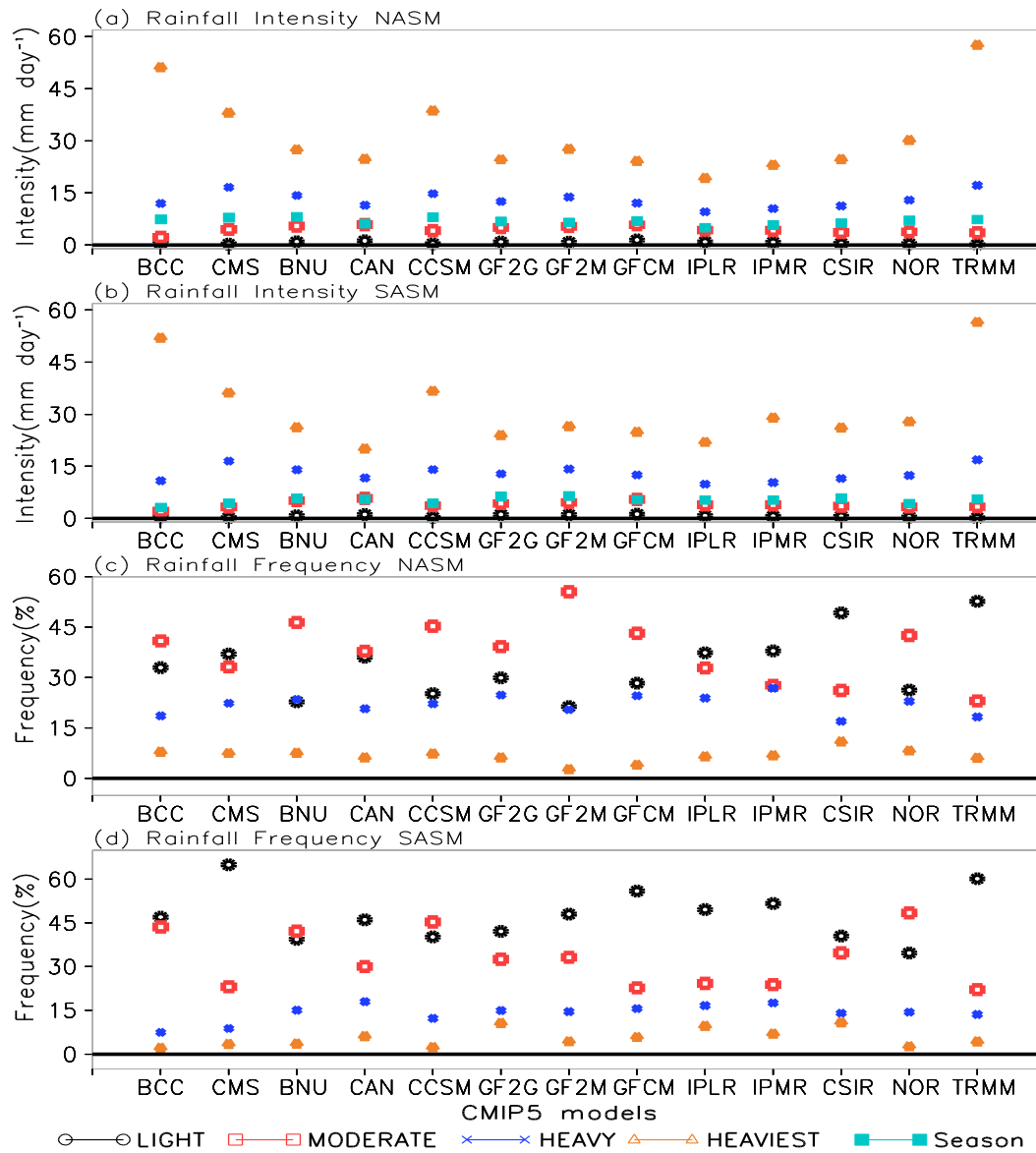


**Figure 4a-d:** Rainfall intensity of various rainfall events over (a) NASM and (b) SASM domains, for historical simulations using 12 CMIP5 models. (c) and (d) are same as (a) and (b), but for rainfall frequency. Here BCC stands for BCC-CSM1.1, similarly CMS for CMCC-CMS, BNU for BNU-ESM, CAN for CanESM2, CCSM for CCSM4, GF2G for GFDL-ESM-2G, GF2M for GFDL-ESM-2M, GFCM for GFDL-CM3, IPLR for IPSL-CM5A-LR, IPMR for IPSL-CM5A-MR, CSIR for CSIRO-Mk3.6.0, and, finally, NOR for NorESM1-M. The unit for intensity is in mm day<sup>-1</sup>, while for frequency, it is in percentages.

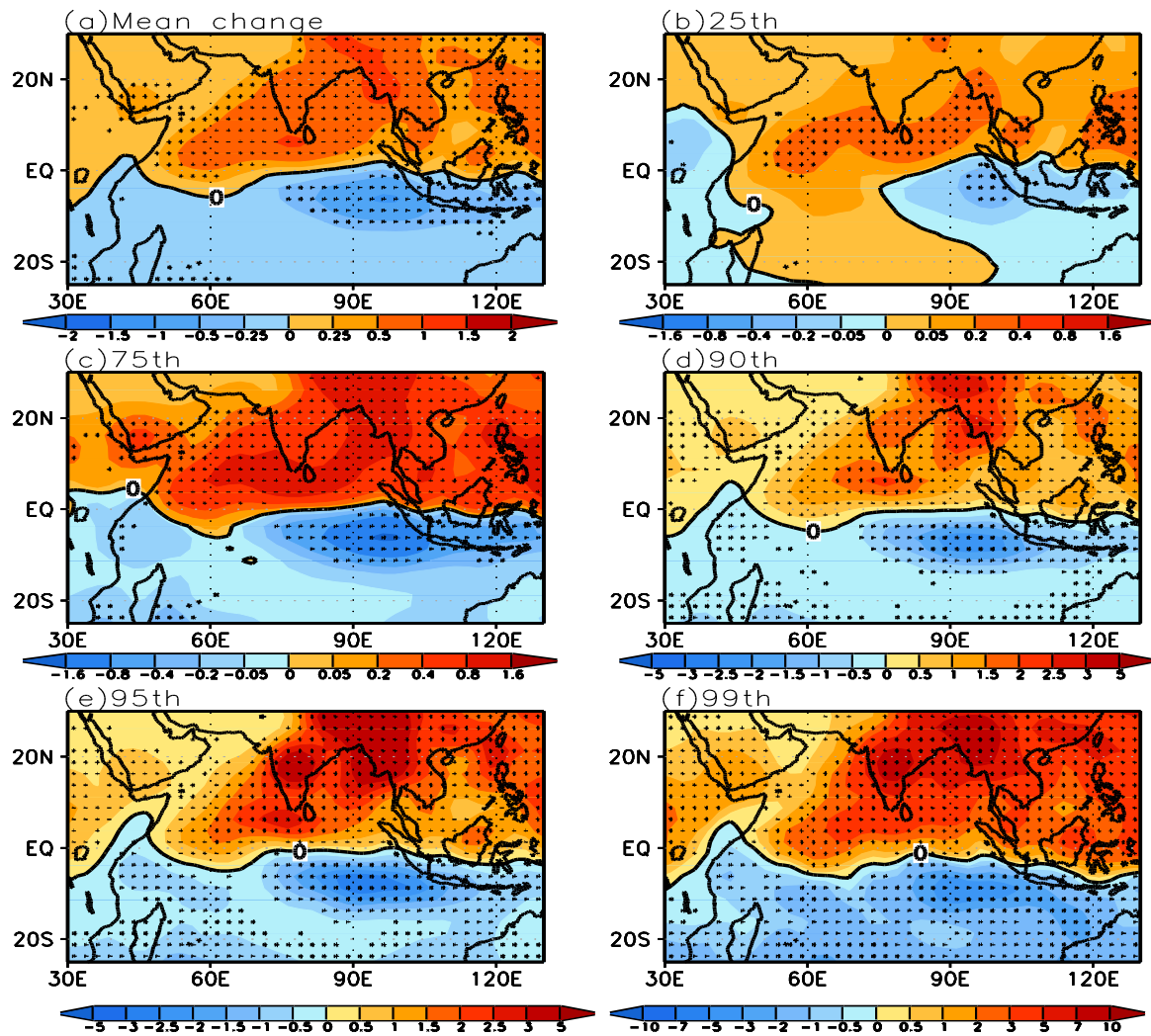


**Figure 5:** Same as that of Figure 2, but for the future rainfall changes. As explained in the text, the rainfall intensities at various percentile thresholds are derived independently for the historical and RCP4.5 simulations and future change is finally calculated. See the text for more details. Stippling denotes the regions of statistically significant values at the 90% confidence level, using a two tailed student *t*-test for the differences of means using a number of degrees of freedom (DOF) of 62 (e.g.  $DOF = 2 \times \text{number of models} - 2$ ). In other words, each model is assumed to be an independent observation for computing the *t*-statistic. Color shading represents the future changes values, without applying any significance test. The thick black contour is the zero isoline.

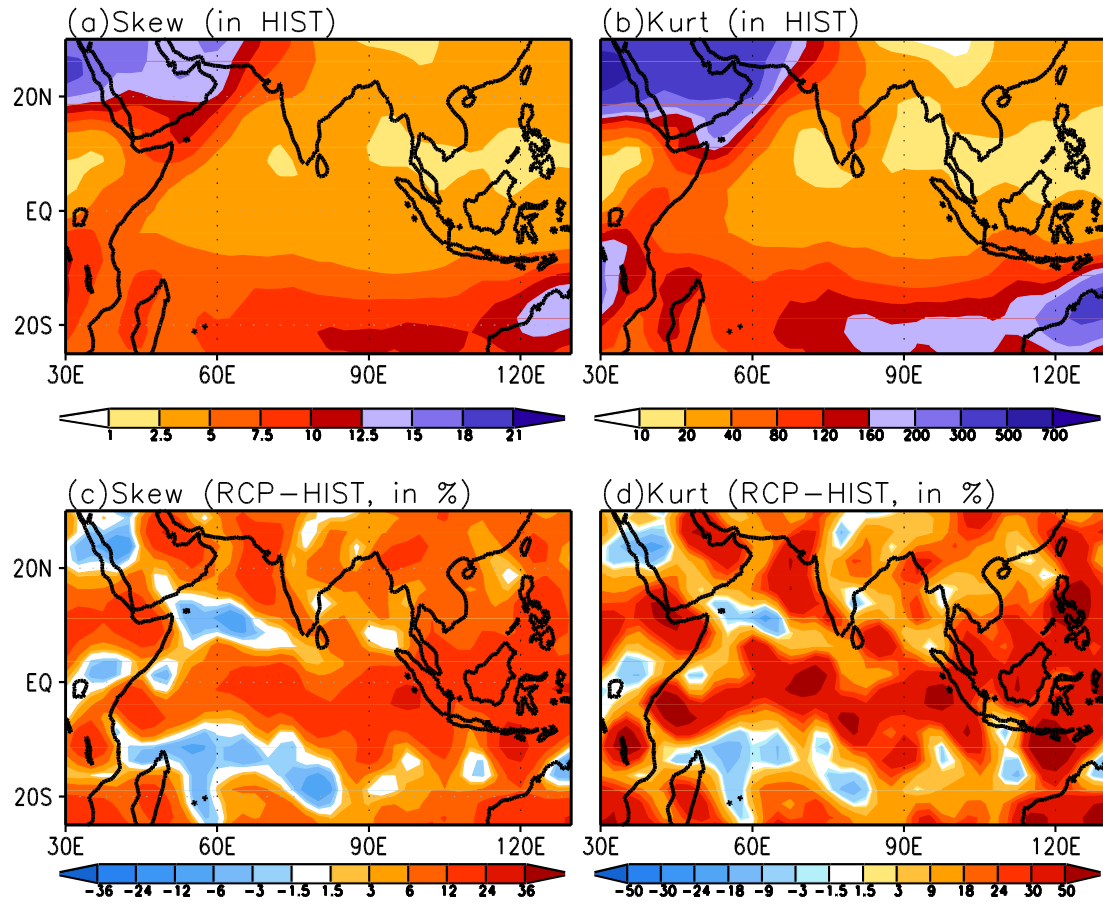


**Figure 6:** Ensemble mean patterns and their future changes for Kurtosis (a and c) and Skewness (b and d) statistics of rainfall distribution, using 32 CMIP5 models. (a) and (b) for present-day climate. (c) and (d) for future change, expressed in percentages.

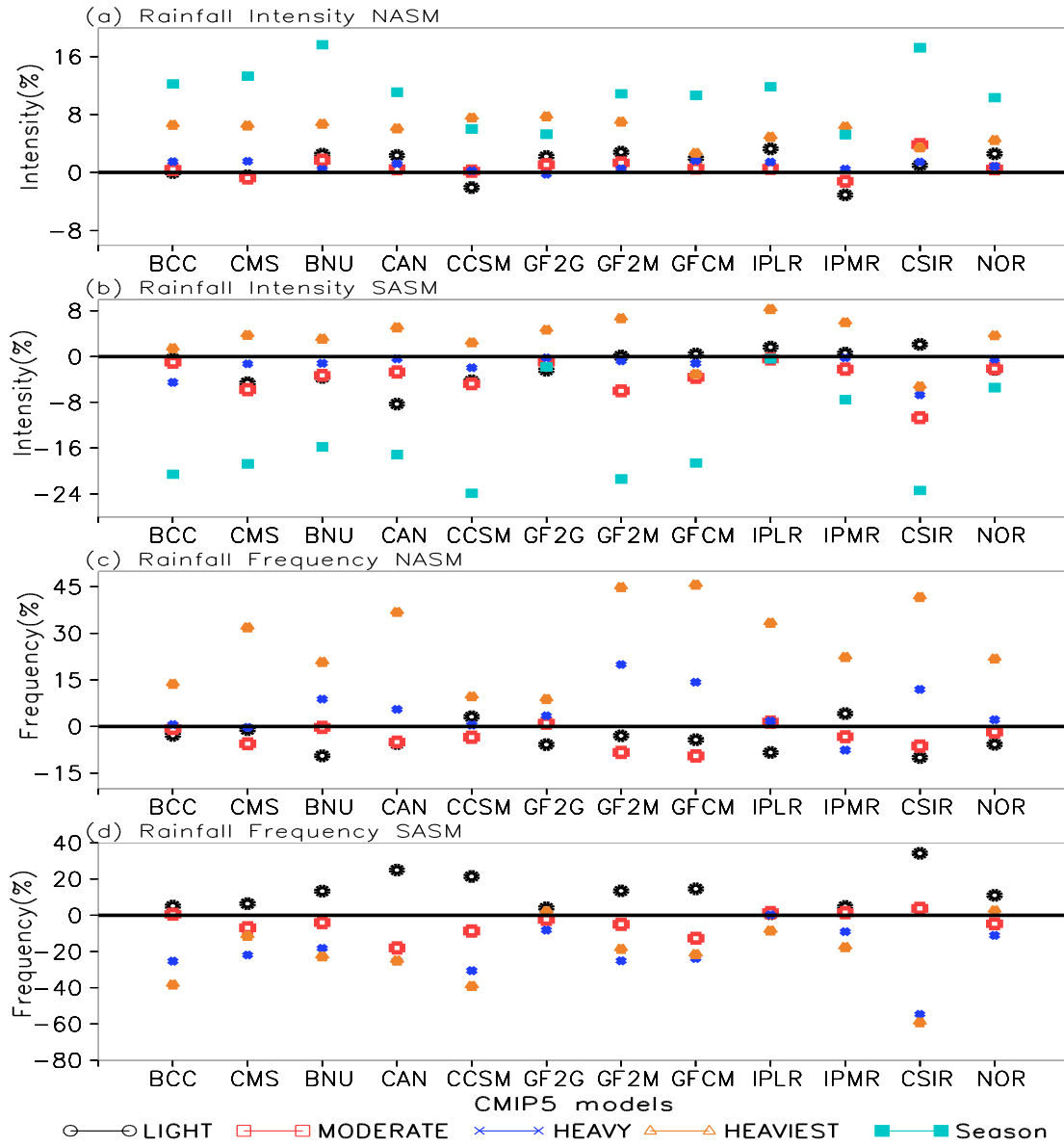


**Figure 7a-d:** Future change in rainfall intensity (in %) of various rainfall events over (a) NASM and (b) SASM domains. (c) and (d) are same as (a) and (b), but for rainfall frequency (in %). Here BCC stands for BCC-CSM1.1, similarly CMS for CMCC-CMS, BNU for BNU-ESM, CAN for CanESM2, CCSM for CCSM4, GF2G for GFDL-ESM-2G, GF2M for GFDL-ESM-2M, GFCM for GFDL-CM3, IPLR for IPSL-CM5A-LR, IPMR for IPSL-CM5A-MR, CSIR for CSIRO-Mk3.6.0, and, finally, NOR for NorESM1-M.

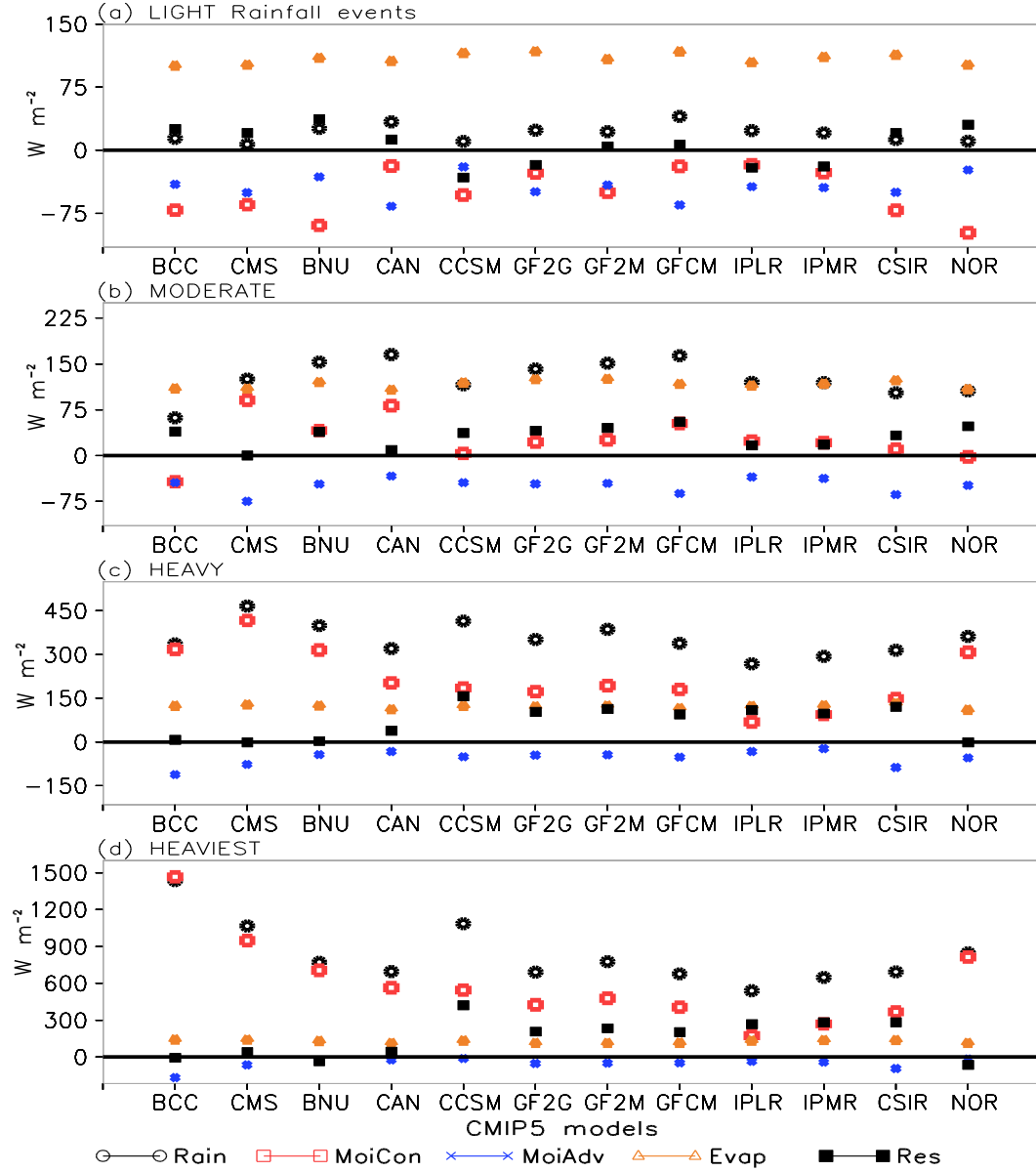


**Figure 8a-d:** Moisture Budget terms (in  $W m^{-2}$ ) over NASM region for the present-day climate, as calculated for various rainfall events. MoiCon represents moisture convergence, MoiAdv is for moisture advection, Evap is for evaporation and Res stands for budget residual term. Here BCC stands for BCC-CSM1.1, similarly CMS for CMCC-CMS, BNU for BNU-ESM, CAN for CanESM2, CCSM for CCSM4, GF2G for GFDL-ESM-2G, GF2M for GFDL-ESM-2M, GFCM for GFDL-CM3, IPLR for IPSL-CM5A-LR, IPMR for IPSL-CM5A-MR, CSIR for CSIRO-Mk3.6.0, and, finally, NOR for NorESM1-M.

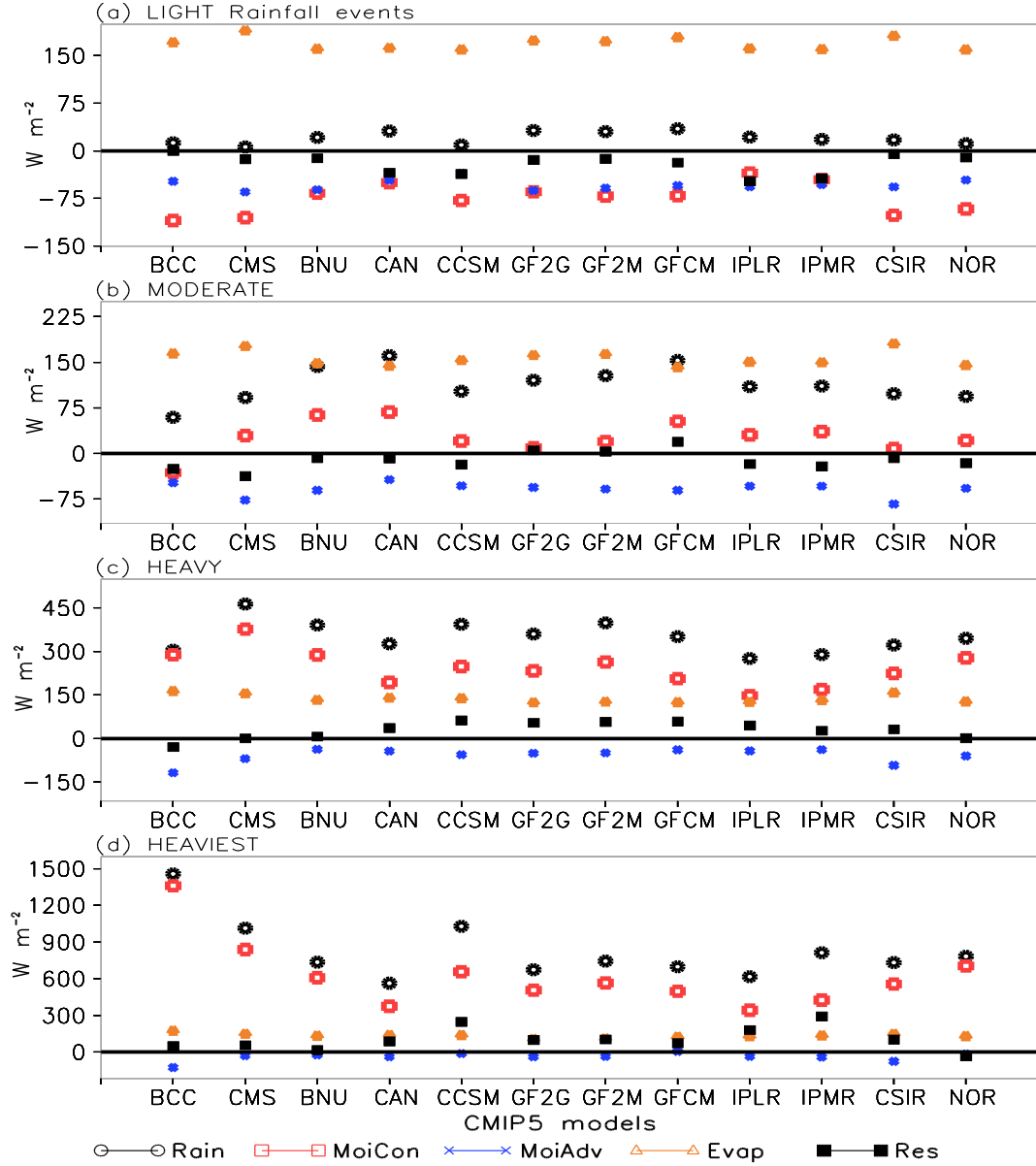


**Figure 9a-d:** Moisture Budget terms (in  $W m^{-2}$ ) over SASM region for the present-day climate, as calculated for various rainfall events. MoiCon represents moisture convergence, MoiAdv is for moisture advection, Evap is for evaporation and Res stands for budget residual term. Here BCC stands for BCC-CSM1.1, similarly CMS for CMCC-CMS, BNU for BNU-ESM, CAN for CanESM2, CCSM for CCSM4, GF2G for GFDL-ESM-2G, GF2M for GFDL-ESM-2M, GFCM for GFDL-CM3, IPLR for IPSL-CM5A-LR, IPMR for IPSL-CM5A-MR, CSIR for CSIRO-Mk3.6.0, and, finally, NOR for NorESM1-M.



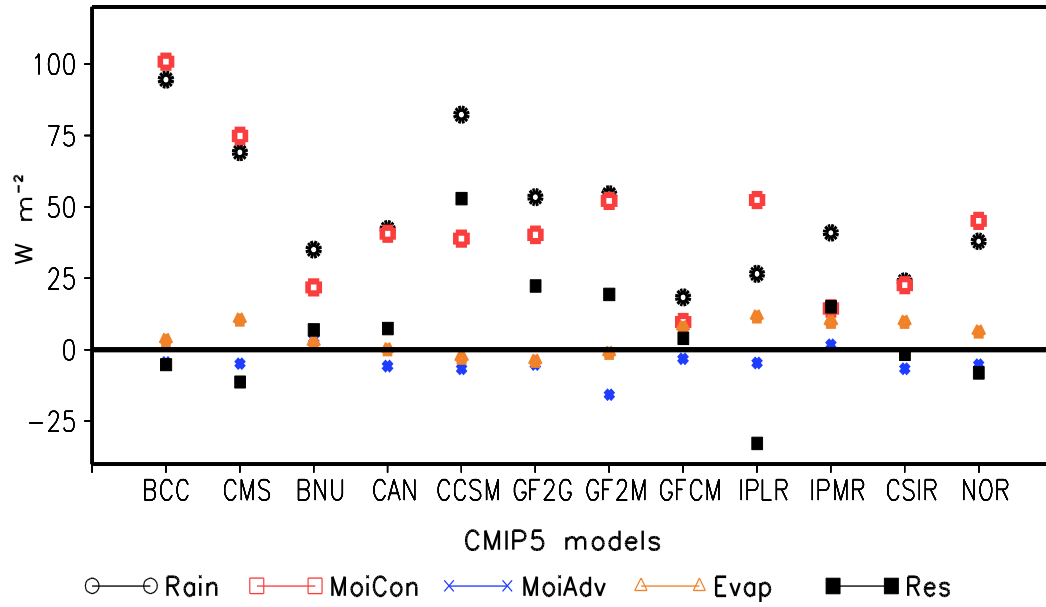


**Figure 10:** Future changes in moisture Budget terms (in  $W m^{-2}$ ) over NASM region as calculated for heaviest rainfall intensities. MoiCon represents moisture convergence, MoiAdv is for moisture advection, Evap is for evaporation and Res stands for budget residual term. Here, BCC stands for BCC-CSM1.1, similarly, CMS for CMCC-CMS, BNU for BNU-ESM, CAN for CanESM2, CCSM for CCSM4, GF2G for GFDL-ESM-2G, GF2M for GFDL-ESM-2M, GFCM for GFDL-CM3, IPLR for IPSL-CM5A-LR, IPMR for IPSL-CM5A-MR, CSIR for CSIRO-Mk3.6.0, and, finally, NOR for NorESM1-M.

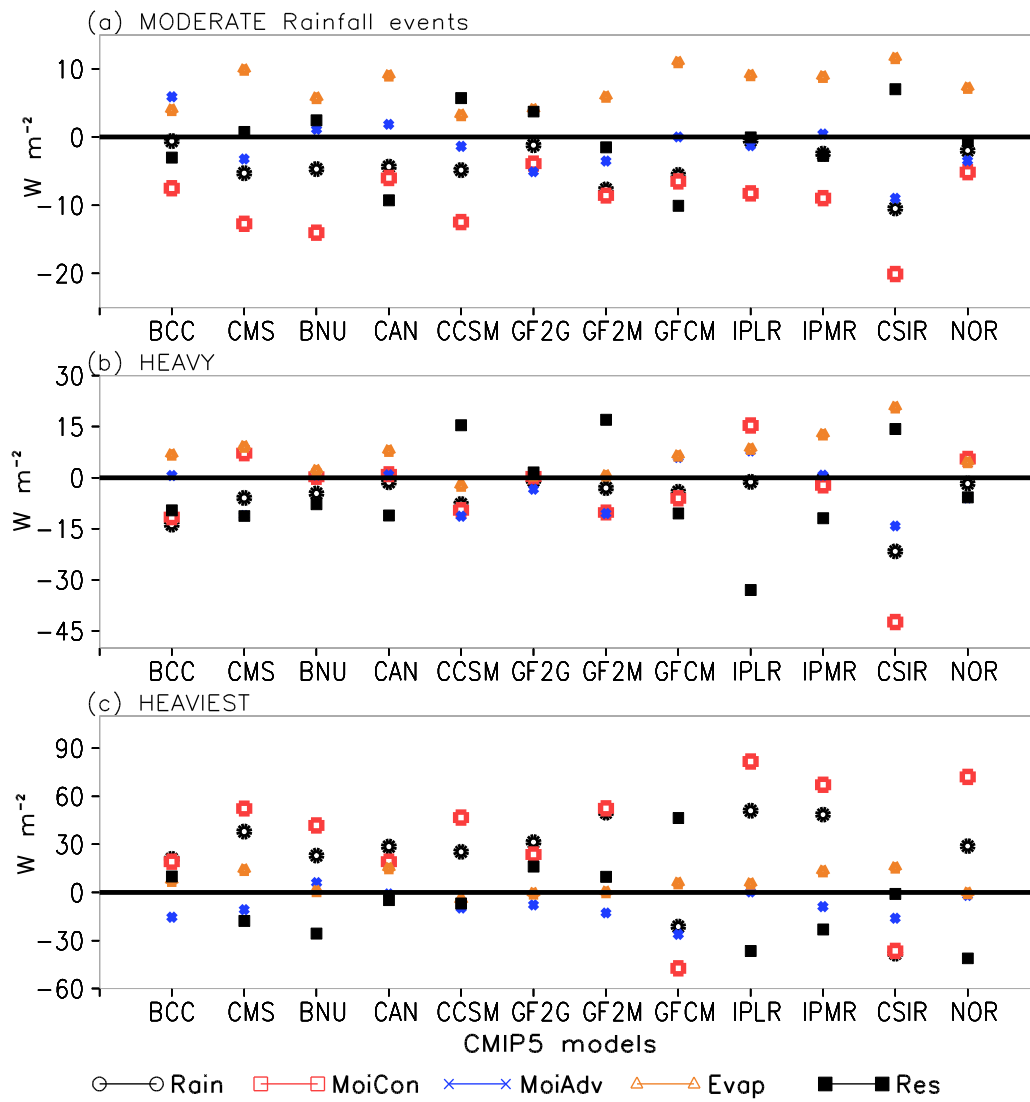


**Figure 11a-c:** Future changes in moisture Budget terms (in  $W m^{-2}$ ) over SASM region as calculated for various rainfall events. MoiCon represents moisture convergence, MoiAdv is for moisture advection, Evap is for evaporation and Res stands for budget residual term. Here, BCC stands for BCC-CSM1.1, similarly CMS for CMCC-CMS, BNU for BNU-ESM, CAN for CanESM2, CCSM for CCSM4, GF2G for GFDL-ESM-2G, GF2M for GFDL-ESM-2M, GFCM for GFDL-CM3, IPLR for IPSL-CM5A-LR, IPMR for IPSL-CM5A-MR, CSIR for CSIRO-Mk3.6.0, and, finally, NOR for NorESM1-M.

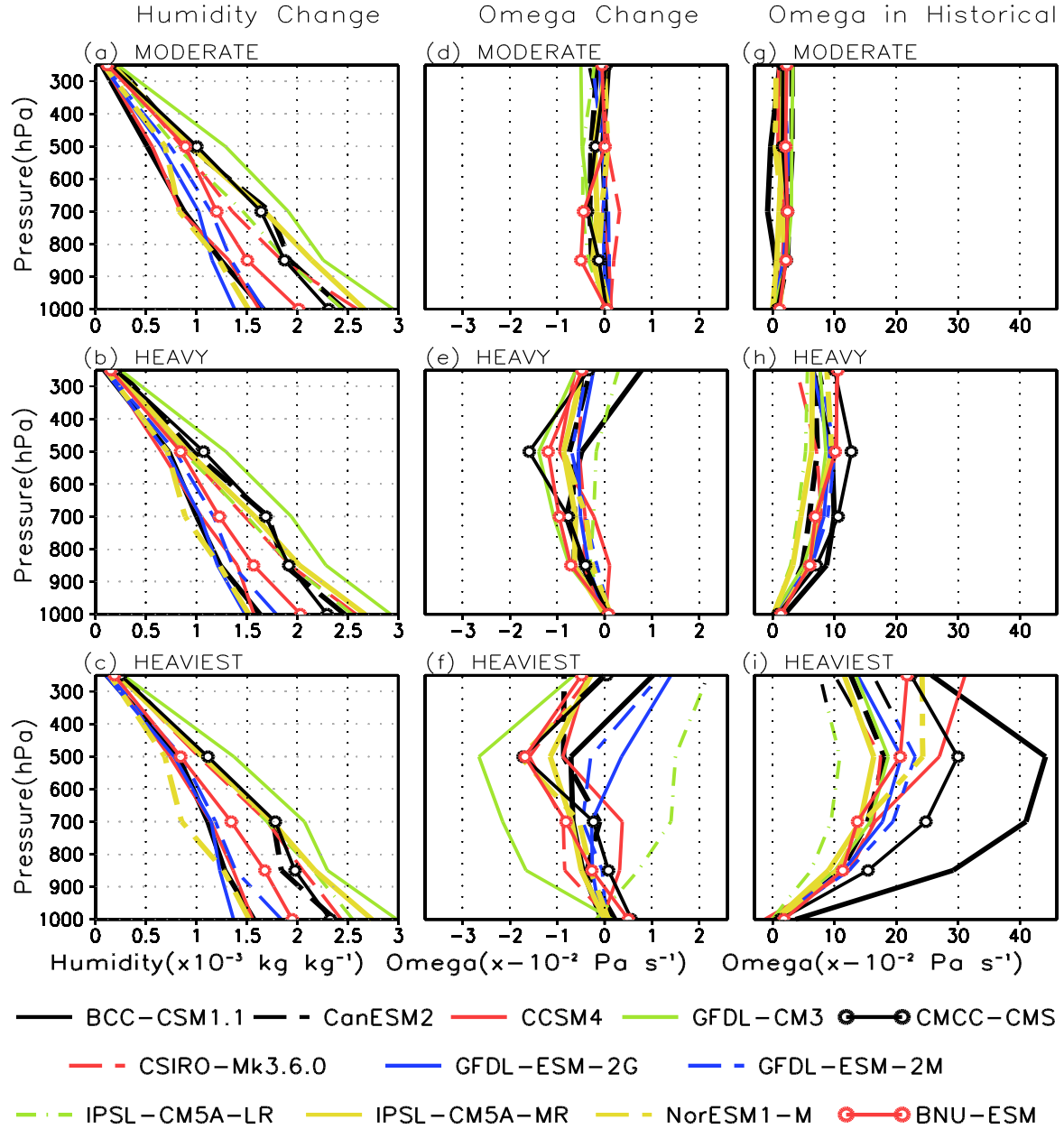


**Figure 12a-f:** (a)-(f) Vertical profiles of future change in specific humidity (left panels,  $\times 10^{-3} \text{ kg kg}^{-1}$ ) and vertical component of velocity (middle panels,  $\times 10^{-2} \text{ Pa s}^{-1}$ ) over NASM, as calculated for various rainfall events in 12 selected CMIP5 models. (g)-(i) Mean vertical profiles of vertical component of velocity (unit is  $\times 10^{-2} \text{ Pa s}^{-1}$ ) computed from historical simulations of the same 12 CMIP5 models, for various rainfall events over NASM.

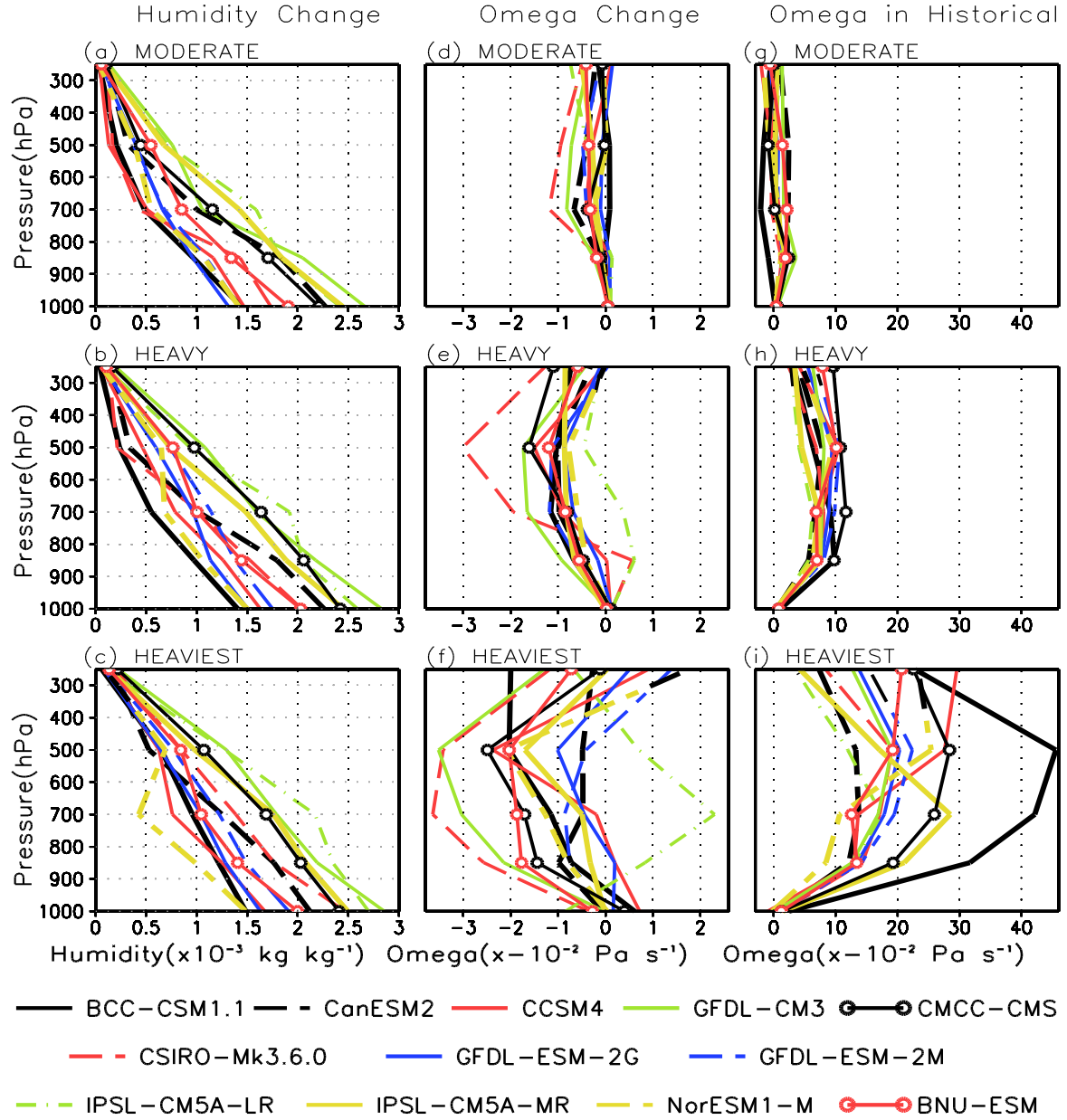


**Figure 13a-f:** (a)-(f) Vertical profiles of future change in specific humidity (left panels,  $\times 10^{-3} \text{ kg kg}^{-1}$ ) and vertical component of velocity (middle panels,  $\times 10^{-2} \text{ Pa s}^{-1}$ ) over SASM, as calculated for various rainfall events in 12 selected CMIP5 models. (g)-(i) Mean vertical profiles of vertical component of velocity (unit is  $\times 10^{-2} \text{ Pa s}^{-1}$ ) computed from historical simulations of the same 12 CMIP5 models, for various rainfall events over SASM.

No.	Couple model name	Institution	Resolution (Lon×Lat, Levels)
1	ACCESS 1.0	Commonwealth Scientific and Industrial Research Organisation and Bureau of Meteorology Australia	192×145, 38
2	ACCESS 1.3	Commonwealth Scientific and Industrial Research Organisation and Bureau of Meteorology Australia	192×145, 38
3	BCC-CSM1.1	Beijing Climate Center, China Meteorological Administration	128×64, L26
4	BCC-CSM1.1(m)	Beijing Climate Center, China Meteorological Administration	128×64, L26
5	BNU-ESM	Beijing Normal University	T42, L26
6	CanESM2	Canadian Centre for Climate Modelling and Analysis	128×64, L35
7	CCSM4	National Center for Atmospheric Research	288×192, L26
8	CESM1-BGC	NSF-DOE-NCAR	288 × 192, 27
9	CESM1-CAM5	NSF-DOE-NCAR	288 × 192, 27
10	CMCC-CM	Centro Euro-Mediterraneo sui Cambiamenti Climatici	T159, 31
11	CMCC-CMS	Centro Euro-Mediterraneo sui Cambiamenti Climatici	T63, 95
12	CNRM-CM5	Centre National de Recherches Meteorologiques and Centre Europeen de Recherche et Formation Avancees en Calcul Scientifique	TL127, 31
13	CSIRO-Mk3.6.0	Commonwealth Scientific and Industrial Research Organisation and Queensland Climate Change Centre of Excellence	192×96, L18
14	FGOALS-g2	Institute of Atmospheric Physics- Tsinghua University	128×60, 26
15	GFDL-CM3	Geophysical Fluid Dynamics Laboratory	144×90, L48
16	GFDL-ESM-2G	Geophysical Fluid Dynamics Laboratory	144×90, L24
17	GFDL-ESM-2M	Geophysical Fluid Dynamics Laboratory	144×90, L24
18	GISS-E2-H	NASA Goddard Institute for Space Studies	144×90, 40
19	GISS-E2-R	NASA Goddard Institute for Space Studies	144×90, 40
20	HadGEM2-AO	National Institute of Meteorological Research/ Korea Meteorological Administration	192×145, 60
21	HadGEM2-CC	Met Office Hadley Centre	192×145, 60
22	HadGEM2-ES	Met Office Hadley Centre	192×145, 38
23	INM-CM4	Institute for Numerical Mathematics	180×120, L21
24	IPSL-CM5A-LR	Institut Pierre-Simon Laplace	96×96, 39
25	IPSL-CM5A-MR	Institut Pierre-Simon Laplace	144×143, 39
26	IPSL-CM5B-LR	Institut Pierre-Simon Laplace	96×96, 39
27	MIROC5	Atmosphere and Ocean Research Institute (The University of Tokyo), National Institute for Environmental Studies, and Japan Agency for Marine-Earth Science and Technology	256×128, 40
28	MIROC-ESM	Japan Agency for Marine-Earth Science and Technology, Atmosphere and Ocean Research Institute (The University of Tokyo), and National Institute for Environmental Studies	128×64, 80
29	MIROC-ESM-CHEM	Japan Agency for Marine-Earth Science and Technology, Atmosphere and Ocean Research Institute (The University of Tokyo), and National Institute for Environmental Studies	128×64, 80
30	MPI-ESM-LR	Max Planck Institute for Meteorology (MPI-M)	T63, 47
31	MRI-CGCM3	Meteorological Research Institute	320×160, 48
32	NorESM1-M	Norwegian Climate Centre	144×96, 26

**Table 1:** Description of the 32 CMIP5 models used in our analysis. The 12 models shown in red are those used for our detailed analysis and those having all the necessary daily atmospheric circulation and precipitation fields in both historical and RCP45 simulations, for conducting moisture budget analysis.